Centro Brasileiro de Pesquisas Físicas

André Carlos Peçanha Lima

Properties of topological chains and electronic correlations

Urca-RJ

2025

ANDRÉ CARLOS PEÇANHA LIMA

Properties of topological chains and electronic correlations.

Tese Apresentada ao Programa de doutorado em Física do Centro Brasileiro de Pesquisas Físicas , como requisito parcial para obtenção do grau de Doutor em Física.

Orientador: Prof. Dr. MÚCIO CONTINENTINO
Co-orientador: Prof. Dr. MARCOS SERGIO FIGUEIRA DA SILVA

Urca-RJ
2025

"PROPERTIES OF TOPOLOGICAL CHAINS AND ELECTRONIC CORRELATION"

ANDRÉ CARLOS PEÇANHA LIMA

Tese de Doutorado em Física apresentada no Centro Brasileiro de Pesquisas Físicas do Ministério da Ciência Tecnologia e Inovação. Fazendo parte da banca examinadora os seguintes professores:

Mucio Amado Continentino - Orientador/CBPF

Marcos Sérgio Figueira da Silva – Coorientador/ CBPF

Rodrigo Arouca de Albuquerque – CBPF

Yutao Xing - UFF

Documento assinado digitalmente
gov.br NILSON ANTUNES DE OLIVEIRA
Data: 22/10/2025 10:18:14-0300
Verifique em https://validar.iti.gov.br

Nilson Antunes de Oliveira – UERJ

Documento assinado digitalmente
gov.br ANDREA BRITO LATGE
Data: 22/10/2025 21:13:36-0300
Verifique em https://validar.iti.gov.br

Andrea Brito Latge - UFF

Rio de Janeiro, 17 de outubro de 2025.

Dedicado ao meu avó Juraci de Souza Lima, que antes que eu pudesse entregar-lhe o resultado de toda uma vida de ensinamentos que compartilhou comigo, partiu de maneira prematura.

Agradecimentos

Agradeço primeiramente a Deus por mais esta conquista, aos meus pais, Márcia Cristina Peçanha Lima Machado e Mauro Neves Machado, por me auxiliarem durante todo o percurso de todas as formas, aos professores Marcos Sérgio Figueira da Silva e Múcio Amado Continentino por toda a atenção e contribuição não somente neste trabalho, mas na minha formação como pesquisador.

Agradeço a minha esposa, Gabriela Fernandes Lima, que permaneceu ao meu lado durante toda a trajetória da minha formação e também me auxiliou das mais variadas formas.

Agradeço ao meu irmão, Arthur Henrique Lima Machado, que sempre esteve disponível nos momentos de dificuldade, aos meus avós, Juraci de Souza Lima e Marlene Peçanha Lima, que estarão eternamente presentes em todas as minhas conquistas, pois tiveram uma enorme importância na formação do meu caráter e a todos aqueles que de alguma forma contribuíram para a conclusão de mais uma importante etapa.

Resumo

Neste trabalho abordamos dois problemas distintos. No primeiro o objetivo é propor sistemas alternativos para a confirmação da existência dos Majoranas. Utilizando das cadeias Su-Schiffer-Hegger(SSH) e Rice-Mele(RM) para a realização de estados de Majoranas-Shockleys sem supercondutividade. Foram estudadas as propriedades termoelétricas e os invariantes topológicos (Winding Number) das cadeias no intuito de verificar se existiam modos de Majorana no sistema. Foi observado que nas cadeias do tipo RM aparecem modos de energia nula mas, no caso específico, são do tipo Majorana-Shockley (MZMSs) que surgem em toda a fase topológica não trivial e na transição de fase do sistema e podem ser observados pelo quantum de condutância elétrica. Além da condutância elétrica outro resultado interessante que vale ressaltar e que corrobora para a existência de cargas fracionárias é o valor do poder termoelétrico a baixas temperaturas. O modo de superfície de energia zero duplamente degenerado torna-se deslocalizado na transição, em todos os locais do sistema incluindo o ponto quântico, tendo assim uma degenerescência dupla. A entropia por sitio é $S = ln2$ e permanece finita em $T = 0$ devido à dupla degeneracência dos estados, quer um sítio seja ocupado por uma partícula ou por um buraco o que implica exatamente nos valores de saturação de baixa temperatura $S = \pm 1.386 \approx \pm 2ln2$.

No segundo trabalho o interesse esta em sistemas topológicos com interação que possam ser resolvidos exatamente. Soluções exatas de sistemas com correlação eletrônica com propriedades topológicas não triviais, embora fundamentais são escassos. Entre os modelos com correlação eletrônica que são solúveis em alguns casos destaca-se a cadeia supercondutora de onda p de Kitaev. Ela desempenha um papel crucial no esclarecimento do aparecimento de quasi-particulas emergentes, os modos de Majorana, seria extremamente útil se fosse possível extende-la incluindo as correlações com o sistema ainda solucionável. foi investigada então uma cadeia supercondutora de Kitaev que interage através de um Hamiltoniano de Falikov-Kimball com um background de elétrons localizados. Para alguns valores dos parâmetros do modelo a solução pode ser obtida, o que permite um estudo detalhado da interação entre correlação eletrônica e comportamentos topológicos não triviais da cadeia.

Palavras chave: Férmions de Majorana, Propriedades termoelétricas, Isolantes topológicos e Coeficientes de transporte.

Abstract

In this work, we address two distinct problems. The first aims to propose alternative systems to confirm the existence of Majoranas. Su-Schiffer-Hegger (SSH) and Rice-Mele (RM) chains are used to realize Majorana-Shockley states without superconductivity. The thermoelectric properties and topological invariants (Winding Number) of the chains were studied to verify the existence of Majorana modes in the system. It was observed that zero-energy modes appear in RM-type chains, but in this specific case, they are Majorana-Shockley modes , which arise throughout the nontrivial topological phase and phase transition of the system and can be observed by the quantum electrical conductance. In addition to electrical conductance, another interesting result worth highlighting and which corroborates the existence of fractional charges is the value of the thermoelectric power at low temperatures. The doubly degenerate zero-energy surface mode becomes delocalized in the transition, at all sites in the system including the QD, thus having a double degeneracy. The entropy per site is $S = ln2$ and remains finite at $T = 0$ due to the double degeneracy of the states, whether a site is occupied by a particle or a hole, which implies exactly the low-temperature saturation values $S = \pm 2ln2 \approx \pm 1.386$.

The second work focuses on interacting topological systems that can be solved exactly. Exact solutions of electron-correlated systems with nontrivial topological properties, although fundamental, are scarce. Among the electron-correlated models that are solvable in some cases, Kitaev's p-wave superconducting chain stands out. It plays a crucial role in elucidating the emergence of emergent quasi-particles, the Majorana modes. It would be extremely useful if it could be extended to include correlations with the still solvable system. A Kitaev superconducting chain that interacts through a Falikov-Kimball Hamiltonian with a localized electron background was investigated. For some values of the model parameters, the solution can be obtained, allowing a detailed study of the interplay between electron correlation and the chain's nontrivial topological behaviors.

Keywords: Majorana fermions, Thermoelectric properties, Transport coefficients, Topological insulators and transport coefficients.

Nomenclature

ABS Andreev Bound State

BBC Bulk-Boundary Correspondence

FK Falikov-Kimball

MF Majorana Fermions

MZM Majorana Zero Modes

OBC Open Boundary Condition

PBC Periodic Boundary Conditions

PF Power Factor

QD Quantum Dot

RM Rice-Mele

SSH Su-Schrieffer-Heeger

STM Scanning Tunneling Microscopy

TEG Thermoeletric Generators

TEM Thermoeletric Materials

$TNSS$ Topological Non-trivial Surface States

WF Wiedemann-Franz

WN Winding Number

ZBP Zero Bias Peak

List of Figures

Contents

Chapter 1

Introduction

In 1937 Ettore Majorana predicted the existence of particles whose antiparticles are themselves by imposing that the Dirac equation described below have real solutions [3].

$$i\big(\gamma^{\mu}\partial_{\mu} - \frac{mc}{\hbar}\big)\psi(x) = 0 \tag{1.1}$$

He obtained this result by using the Dirac equation to study neutrinos. Originally, his proposal was to consider that neutrinos should be described as MF. One of the main interests in the realization of MF is in their use for the construction of quantum bits, since, as the states are topologically isolated, that is, spatially separated and free from any changes originating from the chain's "bulk", they thus allow the storage of information immune to quantum decoherence effects. Quantum information is stored globally (not in local bits), protecting it from local errors.

In 2001, Alexei Kitaev proposed a toy model that enabled the realization of MFs in one-dimensional systems [4] in the Appendix D this model is studied in more detail. However, experimental verification was required to confirm this theoretical prediction. In 2010, Oreg-Lutchyn proposed a setup for the experimental implementation of Kitaev's model [5,6], which are a nanowire with strong spin-orbit coupling, to break energy-level degeneracy, a magnetic field is applied parallel to the wire, to remove residual degeneracy and polarize the energy bands and proximity coupling to an s-wave superconductor, allowing single Cooper pairs to undergo Andreev reflection in the nanowire, forming triplet pairs.

Subsequently, two key experiments sought to observe these Majorana states. The first was conducted by the L. P. Kouwenhoven group in 2012 [1], using an indium antimonide (InSb) nanowire—which exhibits strong spin-orbit coupling—in contact with an s-wave superconductor made of niobium-titanium nitride (NbTiN), under a parallel magnetic field. In this system, a Kitaev chain is believed to have formed at the nanowire-superconductor as can be seen in the figure 1.1. They observed a conductance peak at zero energy, consistent with theoretical predictions for Majorana fermions.

The profound connection is not merely phenomenological; it is deeply rooted in the universality of topological physics. As elegantly demonstrated in unifying works like that of Sato *et al.* [7], the low-energy physics of a wide class of systems—from polyacetylene chains to topological superconductors—is governed by the same fundamental Hamiltonian. The experimental setup of the Kouwenhoven group

realizes a physical incarnation of the Kitaev chain, making the abstract concept of a Majorana fermion a measurable reality.

To build an intuition for this remarkable correspondence, let us deconstruct both systems.

- **The Kitaev Chain:** This is a *theoretical* model of a 1D p-wave superconductor. Its topology is controlled by two key parameters: the chemical potential μ, which determines the electron filling, and the p-wave pairing strength Δ. The system enters a topological phase with end-localized Majorana zero modes when $|\mu| < 2t$, where t is the hopping amplitude.

- **The Kouwenhoven Nanowire:** This is an *experimental* platform consisting of a semiconducting nanowire (e.g., InSb) with strong spin-orbit coupling, placed in a magnetic field B, and in proximity to an s-wave superconductor (e.g., Aluminium). The key parameters here are the Zeeman energy $V_Z = g\mu_B B/2$ and the chemical potential μ.

The conceptual leap, formalized in the work following Sato's insights, is to recognize that these two systems are described by mathematically equivalent Hamiltonians. The mapping between them is both elegant and powerful.

The Kitaev model requires spinless fermions to achieve p-wave pairing. In the nanowire, this is ingeniously engineered. The combination of strong spin-orbit coupling and an external magnetic field lifts the spin degeneracy, creating two distinct sub-bands. By tuning the chemical potential to the bottom of one of these bands, the low-energy physics is effectively governed by a single species of *helical*, or effectively spinless, fermions.

The Kitaev model assumes intrinsic p-wave pairing (Δ). The nanowire itself is not a p-wave superconductor. However, the proximity effect induces superconducting correlations from the s-wave parent superconductor. Crucially, the spin-orbit interaction and the magnetic field *transform* these induced correlations. For the effectively spinless electrons, the induced pairing appears as an effective p-wave gap. The magnitude of this effective gap is proportional to the parent s-wave gap and depends on V_Z and the spin-orbit strength.

In the Kitaev chain, the transition occurs at $|\mu| = 2t$. In the nanowire, the equivalent condition is $V_Z > \sqrt{\mu^2 + \Delta_{\text{ind}}^2}$. When this inequality is satisfied, the system enters the topological phase. The applied magnetic field B is the experimental "knob" that tunes the system across this topological quantum phase transition.

From Toy Model to Testable Prediction elevates the Kitaev chain from a pedagogical toy model to a quantitative tool for predicting experimental outcomes. The celebrated zero-bias conductance peak (ZBCP), observed by Kouwenhoven, is a direct experimental signature of the Majorana zero mode predicted by the Kitaev model's end states. Universality of Topological Physics It demonstrates that the core physics—the emergence of non-Abelian anyons at phase boundaries—is robust. It does not depend on the microscopic details of the system but on the universal topological class to which it belongs. The nanowire and the Kitaev chain are siblings in the same topological family. A Guide for Material Design equivalence provides a clear recipe for engineering topological superconductivity. It tells us that the

essential ingredients are spin-orbit coupling, a magnetic field, and s-wave superconductivity, guiding the search for new material platforms.

Therefore, the experiments of the Kouwenhoven group are not just a tentative observation; they are a direct and sophisticated validation of the Kitaev chain's core principles, translated into a semiconductor heterostructure. In this chapter, we will delve into the details of this mapping, explore the resulting band structure, and derive the key experimental signatures that link the abstract beauty of topology to the concrete world of measurable quantum phenomena.

In Figure A one can see that the nanowire with strong spin-orbit interaction promotes a transverse magnetic field $\vec{B}_{SO}$ that laterally shifts the energy bands (blue and red curves) thus breaking the degeneracy, so that there is still a degeneracy that is broken when one cross a magnetic field that also aligns the energy bands(black curves). Figure B is an image of the experiment carried out by Kouwenhouven's group, where S is the superconductor, the white line is the nanowire, N is a conductive material (gold) used as a reservoir and $\vec{B}$ is the magnetic field.

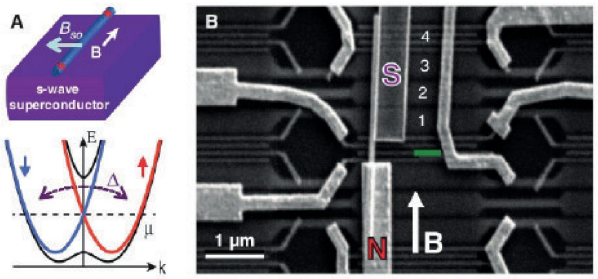

Figure 1.1: Experiment conducted by L.P. Kouwenhoven's group [1].

One of the significant challenges in the experimental detection of MF in condensed matter systems is the potential interference from magnetic impurities (known as Shiba states), structural or chemical defects, and conventional states (like Andreev states). These factors can produce signatures that closely resemble those expected for Majorana Fermions, leading to controversies in the interpretation of various experiments.

The measurement process can produces conductance signals associated to impurities and Majorana zero modes conductance peaks can appear at zero energy in STM/transport experiments [8]. Andreev states can be trapped in imperfections or disorder in the material, mimicking the expected location of MZM [9]. Magnetic impurities like Shiba states which are bound quantum states that arise when magnetic impurities (such as iron or manganese atoms) are inserted into a superconductor also generate similar peaks. Their presence can create zero-energy spikes indistinguishable from Majoranas without additional measurements of conductance and response to external disturbances [2, 8] in defects in the material or non-uniform couplings. Imperfections in nanowires can create localized ABS at the ends, mimicking the expected spatial signature for MZMs [10].

The second experiment, performed by Ali Yazdani's group in 2014 [11], involved a ferromagnetic chain with aligned spins deposited on a lead (Pb), an s-wave. The chain's conductance was measured using a STM as one can see in figure 1.2.

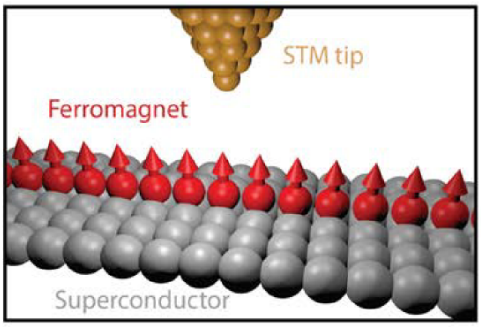

Figure 1.2: STM used in measuring chain conductance [2]

In 2014, the Ali Yazdani group investigated the existence of Majorana fermions in atomic chains of iron (Fe) deposited on a superconductor (Pb) using STM to detect bound states at zero energy at the ends of the chains. Peaks of density of states at zero energy were observed, located at the ends of the chains, compatible with MZMs. Exclusion of artifacts (Andreev states) was done via analysis of magnetic field dependence and theoretical simulations, thus obtaining robust experimental evidence of MZMs in a clean and controllable system. However, once again the results could be associated with disorder and impurity effects, since the presence of impurities in the Fe chains or in the Pb substrate could create spurious states, mimicking Majorana signatures [2].

Another experiment performed by Zhang's group, in 2018 [12], investigates the formation of MBSs in a system combining semiconductor nanowires (InSb) with coupled quantum dots aiming to distinguish MBS from spurious states. However, the group had to retract [13] their findings after the results were questioned due to spurious effects, that is signals that mimic the expected signatures of Majorana Fermions, as Andreev states, but originate from conventional non-topological phenomena that were not taken into account. New, more precise data, collected by their own group and others, showed that an identical signal could be produced by a more trivial and conventional physical phenomenon, not requiring Majorana particle physics. The group reported finding strong evidence for Majorana fermions in a system of superconducting iron-lead nanowires.

Another work of 2025 [14], proposes a method for measuring fermionic parity (an indicator of Majorana states) in InAs-Al (indium arsenide–aluminium) hybrid devices using a single-shot interferometry technique. This approach aims to distinguish MZMs from spurious states such as ABS, with high accuracy, but, the experiment also has false positives generating an irregular response or one dependent on local disorder.

Irregular response of spurious states, refers to fluctuations in the conductance of conventional states (ABS, Shiba). That can exhibit peaks at $\omega = 0$ that disappear or change energy with small variations in the magnetic field or electric gate and do not show the robust quantization ($2\frac{e^2}{h}$) expected

for Majoranas and chaotic dependence of parameters as in real devices (such as InAs-Al nanowires). Impurities or disorder cause the conductance peaks to appear in random positions along the wire not just at the ends and have variable widths and heights, differing from the clean signature of Majoranas.

In superconducting systems, parity is a topological property associated with MZMs. Non-Abelian Majorana states allow robust parity operations, while conventional states (ABS, impurities) do not. It is worth noting that spurious states are a subset of conventional states and are defined as any conventional state that mimics Majorana signatures, leading to false positives. These include quasi-degenerate ABSs at $\omega = 0$, Shiba states at zero energy, and disorder-localized modes.

The experiments that were performed to detect MZMs have presented limitations that leave their results inconclusive, in confined systems such as quantum junctions and disordered nanowires, multiple Andreev reflections can create steady states called ABS [15, 16] within the superconducting band gap ($E < \Delta$). In a weakly coupled junction (e.g., a quantum dot between two superconductors), electrons and holes are "trapped" in resonances, forming Andreev bound pairs. These states have discrete energies (E_{ABS}) that depend on the superconducting phase (ϕ) and the coupling. Under certain conditions (e.g., high transparency of the junction), an ABS can approach zero energy ($E_{ABS} \approx 0$), simulating a MZM.

ABS are localized and therefore vulnerable to fluctuations and are non-topological, while MZMs are non-local and protected by topology. The quantum information in a topological qubit is stored in the entire system, not at a specific point, it is worth highlighting that in systems proposed to host Majorana fermions, can supress or modify [17], since both Kondo and Majorana states produce conductance peaks at V=0, are sensitive to temperature (T), but Majoranas are topologically protected [18].

Imperfections in the interface between the semiconductor and the superconductor can distort the induced superconducting gap, creating spatial variations, introducing disorder into the system, affecting the stability and detection of Majorana fermions [19].

The effective gap (Δ_{eff}) is the crucial parameter for the formation of topological states, such as Majoranas, as it defines an energy scale where they appear, if the obstruction between the materials is not homogeneous or perfect, regions with higher Δ_{eff}, lower or even zero may appear. Contamination or oxidation by impurities (e.g. oxides) between the materials prevents the efficient transfer of Cooper pairs, which causes non-ideal bonding, or even poor adhesion or mechanical stress, that is, if the semiconductor is not perfectly bonded to the superconductor, the coverage becomes irregular, or even intrinsic disorder in the semiconductor [6].

Non-uniform crystal defects or doping affect superconducting proximity as a consequence of disorder. Regions with $\Delta_{eff} \approx 0$ appear that act as "non-superconducting islands", where electrons can be trapped, creating localized ABSs and low-energy states that mimic Majoranas [10]. The topological phase which hosts Majoranas, requires a uniform and well-defined gap, if Δ_{eff} varies in space, parts of the system may not be in the topological phase causing topological inhomogeneity, destroying the protection of the MZMs and experimental difficulty because transport measurements e.g. conductance at zero bias are ambiguous. So that peaks may come from ABS in regions with $\Delta_{eff} \approx 0$ and genuine Majoranas may not form due to lack of coherence in the gap.

In the first case, p-wave superconductors (required for unambiguous MF) are rare in nature and highly sensitive, meaning the observed signals could stem from disorder or impurities. In the second case, the Kondo effect could supress or modify the Majorana fermion signatures. An alternative approach to confirming these states was proposed by Liu and Baranger in 2011 [20], suggesting a detection method using a quantum dot (QD).

The Zhang group, in the 2018 [12], used a STM tip to spectroscopically measure the energy states within the nanowire and observed a conductance peak precisely at zero energy called the Zero Bias Peak - ZBP. In theory, this peak is the expected "signature" of a Majorana quasi-particle, which appears at the ends of the nanowire. In the years that followed, two main questions arose: the most crucial property of a true Majorana mode, besides the lack of "robustness" (quantization plateau), is that, the signal (the height of the conductance peak) must be quantized to a specific, universal value ($\frac{2e^2}{h}$) and must be robust, it must not disappear with small variations in parameters such as magnetic field or voltage. The signal observed by the group was not robust; it fluctuated and did not stabilize at the expected quantized value. This raised initial suspicions, as did the fact that ABS could produce a zero-energy peak that was virtually indistinguishable from the signal they had attributed to a Majorana. In the new paper [13], they essentially admitted that the 2018 interpretation was weak and concluded that the signal they observed was compatible with a pair of accidentally degenerate ABS at zero energy, not a robust topological Majorana mode. The scientific community took this as a de facto retraction of the previous claims.

Topological one-dimensional superconductors can sustain zero energy modes protected by different kinds of symmetries. Observing these excitations in the form of Majorana fermions is one of the most intensive quests in condensed matter physics. We are interested in another class of one-dimensional topological systems namely topological insulators. Topological insulators are a class of quantum materials that combine insulating properties in the bulk (interior) with conducting states at their edges or surfaces. These surface states are topologically protected, that is, they are robust against local disturbances such as impurities or disorder, as long as certain symmetries of the system are preserved. Its discovery revolutionized condensed matter physics, uniting concepts of topology and electronic physics that present symmetry-protected final modes with robust properties and that do not require the low temperatures necessary for topological superconductivity.

In Chapter 2, in the Sec. 1, 2 and 5, we consider a device in the form of a single electron transistor coupled to the simplest kind of topological insulators, namely chains of atoms with hybridized sp orbitals. We study the thermoelectric properties of the device in the trivial, non-trivial topological phases and at the quantum topological transition of the chains in the Sec. 6. We show that the device's electrical conductance in the Sec. 7 and the Wiedemann-Franz ratio at the topological transition have universal values at very low temperatures in the Sec. 9. The conductance and thermopower of the device with diatomic sp-chains, at their topological transition, give direct evidence of fractional charges in the system in the Sec. 8 and 9. The former has an anomalous low-temperature behavior, attaining a universal value that is a consequence of the double degeneracy of the system due to the presence of zero energy modes.

On the other hand, the system can be tuned to exhibit high values of the thermoelectric figure of merit and the power factor at high temperatures in the Sec. 10 and 11, from these results we consider carrying out a more in-depth study of the system when in the non-trivial topological phase.

Most studies of non-trivial topological systems are carried out in non-interacting models that admit an exact solution. This raises the question, to which extent the consideration of electronic correlations and disorder, present in real systems, modify these results. Exact solutions of correlated electronic systems with non-trivial topological properties, although fundamental are scarce. Among the non-interacting soluble models, we single out the Kitaev p-wave superconducting chain already studied initially in the present work. It plays a crucial role in clarifying the appearance of emergent quasi-particles, the Majorana modes, associated with non-trivial topological properties. Given the relevance of this model, it would be extremely useful if it could be extended to include correlations and still remain solvable thinking about it in this work we investigate also a superconducting Kitaev chain that interacts through a FK Hamiltonian with a background of localized electrons [21]. For some relevant values of the parameters, this model can be solved exactly by mapping into a non-interacting one. This allows for a detailed study of the interplay between electronic correlations and non- trivial topological behavior. Besides, the random occupation of the chain by the local moments brings new interesting effects associated with disorder.

Systems with non-trivial topological properties have been the subject of intensive studies in recent years [3,4,22–25]. They have expanded the landscape of interesting materials in the periodic table, giving rise to new concepts and to the discovery of unsuspected physical properties. Theoretical study of models with non-trivial topological properties has in many cases anticipated unusual behavior, creating exciting challenges to experimentalists. A clear example is the Kitaev superconducting chain model with emergent new quasi-particles, the Majorana fermions, on its edges [4]. The unusual properties of these modes [25–30] is leading to enormous progress in experimental nano-physics [3,5,23–25,31–39].

Many of the models of topological superconductors and insulators are idealized, since they do not include electronic correlations or disorder, and consequently can be solved exactly. In one aspect this is satisfactory, since it allows to obtain a clear picture of the nature of the emerging quasi-particles and topological non-trivial properties. On the other hand, it raises the question to which extent these properties are robust to electronic correlations, or disorder, present in real materials [40–45]. The motivation of the present study is to explore this problem presenting a non-trivial topological interacting model with an exact solution for some values of its parameters.

Models describing Majorana fermions in topological systems often assume non-interacting particles. However, interactions between fermions can generate spurious effects, creating localized zero-energy states that mimic Majoranas, even in non-topological systems [46]. Furthermore, strong interactions can destroy or create new topological phases, confounding the detection of genuine Majoranas, such as in superconducting nanowires, which have electronic interactions that can induce confined Andreev pairs that hybridize with edge modes, producing peaks at E=0 indistinguishable from Majoranas in scanning tunneling spectroscopy.

Interactions can lead to false positives through modified Kondo states because quantum dots

coupled to superconductors, strong interactions between electrons and magnetic impurities generate resonances at E=0 and correlated disorder, that is, interactions between defects create random potentials that localize trivially confined states [47].

The FK model plays an important role in the study of strongly correlated systems, as heavy fermions and mixed-valence material [21, 48, 49]. The model consists of a conduction band of itinerant electrons interacting with a background of localized electrons. In this paper we obtain an exact solution for the one-dimensional spinless FK model with a p-wave pairing of the electrons in the conduction band.

The solution is possible since we can formally map the many-body problem in a non-interacting system with a site dependent chemical potential [50–52], although our problem has two types of electrons. We consider three cases: homogeneous, staggered, and disordered configurations of the local moments. The motivation is that these phases will have different signatures when we turn on the p-wave superconducting interaction between the conduction electrons.

Systems with exact solutions often consider models where electrons can be localized in discrete sites, such as in one-dimensional chains or lattices. Electron localization allows for the definition of well-characterized creation/annihilation operators, which are the basis for constructing Majorana operators. With localized electrons, it becomes possible to derive exact Majorana modes and study their robustness to perturbations and interactions, which is crucial for differentiating genuine modes from spurious states. Furthermore, the exact description facilitates the analysis of the system's topology, precisely identifying regions where Majorana modes appear, such as at the ends of chains or at topological interfaces.

The presence of localized electrons creates ideal conditions for the formation of localized Majorana modes that can be detected experimentally [53]. These modes can be observed through electronic transport measurements (such as ZBP conductance) at specific points where electrons are confined. Control over localized electrons also allows the manipulation of Majorana modes for braiding operations, essential for applications in topological quantum computing. Systems that exploit localized electrons with exact solutions increase detection accuracy by reducing noise and ambiguities caused by spurious modes.

In the Chapter 3 our work allows to explore on firm ground the interplay between electronic correlations and non-trivial topology [54]. Since the local moments can randomly occupy the sites in the lattice, we also consider the effect of disorder on the interacting topological system.

We organize the chapter in the following way: In the Sec. 1 we define localized electrons, in Sec. 2, we introduce the Hamiltonian, which is a generalization of the p-wave superconducting Kitaev chain [4], to include an interaction of the conduction electrons with a background of localized electrons through a FK Hamiltonian [21]. In Sec. 4, we present the formalism and the exact solution of the model. In Sec. 5, we briefly discuss the properties of the pure one-dimensional spinless FK model, since this will be useful to characterize the superconducting phases. Sec. 7 treats the general case of a conduction band with a p-wave pairing that interacts with localized f-electrons. We obtain the dispersion relations and density of states of infinite chains. For a full characterization of the topological properties we investigate numerically the appearance of MZMs in finite chains with open boundary conditions, including the case

the local moments are randomly distributed. In Sec. 7 we study in detail random chains, with different probabilities of occupations of the sites by local moments. This allow to examine the effects of disorder in the topological properties. Finally, in chapter 4 we conclude with a summary of our results and a discussion on new perspectives and extensions of the model.

Chapter 2

Thermoelectric properties of topological chains coupled to a quantum dot

The origin of *thermoelectricity* can be traced back to the discovery of the Seebeck effect in the 19^{th} century. It consists in the production of electrical energy directly from heat, and its inverse, the Peltier effect, that transforms electrical energy into thermal energy. After the development of the first TEGs with applications in industry [55], these lost the competition with the dynamoelectric machines due to the high costs of their electrical energy generation. Their technological development was interrupted for several decades. Only in the middle of the last century, due to the needs of the aerospacial and military industries, did the interest in developing new TEGs reappear. The thermoelectricity acquires some practical applications in those strategic areas after the discovery that the doped semiconductor Bi_2Te_3 and its alloys Sb_2Te_3, and Bi_2Se_3 [56–58], present high electric conductivities σ and low thermal conductivities κ. In consequence, those TEM exhibit at ambient temperatures a higher dimensionless thermoelectric figure of merit (zT) [55, 56] and a high PF and, until now, dominate the commercial industry of TEGs [59].

Recently, it was shown that the usual TEM, like Bi_2Te_3, Bi_2Se_3, Sb_2Te_3, and $FeSb_2$ [60–62] are also three-dimensional topological insulators exhibiting surface states with a single Dirac cone and some of their striking properties are due to their strong spin-orbit coupling [59, 63, 64] and their conducting surface states [65, 66]. A promising route to explore the effects of the TNSS on the TE properties was followed in Ref. [67], which studied thin films of Bi_2Te_3. The authors used first-principles calculations and Boltzmann theory to obtain zT for different film thicknesses. They defined a unit of quintuple layers (QL) of the real material $Te - Bi - Te - Bi - Te$ and observed a $p-$type and $n-$type $zT \simeq 2$ peak in $QL = 3$ when the system enters the topologically non-trivial regime from the trivial one. The results show a relevant enhancement of zT due to the contribution of TNSS compared to the pristine form of bulk Bi_2Te_3, $zT = 0.4$. Another step in the direction of the use of TNSS states in real systems was obtained after the recent advances in the synthesis of Bi_2Te_3 thin films, which allows separating the bulk from the TNSS states in order to design quantum devices with improved thermoelectric properties [68].

The study of topological systems is now one of the most active areas of research in condensed matter physics [3, 40, 69, 70]. The theoretical efforts to understand the properties of these systems has lead to the predictions of emergent excitations with unexpected properties that make them potentially useful for different types of applications. Among these works, Kitaev model for a p-wave superconducting chain [4] has played a fundamental role and many suggestions have appeared of how to realize this model in actual physical systems. In the topological phase, the finite one-dimensional Kitaev superconducting chain presents Majorana, zero energy modes, at its ends. The physical implementation of the p-wave Kitaev model and the detection [1,5,6,17,22,71–74] of the zero energy Majorana modes is a modern Graal in materials research. In this pursuit an initial major difficulty is to obtain a p-wave superconductor, since this is far from being common in nature [75]. Several proposals have been put forward to generate this type of pairing in a chain, mostly using proximity effects and magnetic fields [3].

Besides one-dimensional p-wave superconductors there is a class of topological insulating [76, 77] chains that is much simpler and also presents protected zero energy modes at their ends. Representative members of this class are sp-chains consisting of atoms with hybridized s and p orbitals [78]. The mixing between s and p orbitals in neighboring ions is antisymmetric and this gives rise to non-trivial topological properties [79], in close analogy with the antisymmetric p-wave paring of the Kitaev chain. Notice that the asymmetry of the mixing holds for any pair of orbitals that have angular momentum quantum numbers differing by an odd number. In spite of their symmetry protection, the edge modes in topological sp-chains have distinct features from the Majoranas in the Kitaev chain. The former are quasi-particles with a hybrid sp-character that are formed of two different types of Majoranas [78].

The sp-chains may be easier to realize in practice then p-wave superconductors. Also, they do not require the low temperatures necessary for superconductivity, to manifest their topological properties. A possible realization of the sp-chain is carbyne, the one-dimensional allotropic form of carbon [76, 80–83]. In this system the $2s$ orbital hybridizes with a *single* $2p$ orbital favoring a linear atomic alignment [84]. A significant effort has been made in the synthesis of these materials that in principal can exist in a metallic state (cumulene) and in an insulating, broken symmetry state, with alternating single and triple bonds [80].

As we show in the appendix monoatomic and diatomic sp-chains can be mapped in two very well known topological chains, the Su-Schrieffer-Heeger (SSH) [85, 86] and the Rice-Mele (RM) [87, 88] chains, respectively. These chains have been intensively studied and their topological properties are well known. For this reason we study here the latter two models since they yield results for the thermoelectric properties similar to those of the sp-chains.

This paper studies the thermoelectric properties of two semi-infinite Rice-Mele chains connected to a quantum dot. We investigate the device's electrical and thermal transport properties as a function of temperature, in the topologically non-trivial and trivial phases and at the topological transition. According to Refs. [67, 68] we expect an increase of zT due to topological states at the edges of these chains.

This work has the following structure: In section 1, we introduce the Rice-Mele model and

present its topological properties. We employ a method developed in Ref. [89] to obtain the local Green's function at the edge of the chain. This yields the *surface* density of states for the Rice-Mele chain. In section 6, we present the device consisting of two identical semi-infinite topological chains connected to a singly occupied quantum dot [90], without correlations effects. We use linear response theory to define the thermoelectric coefficients. In sections 6 and 7 we calculate, electrical and thermal conductances, thermopower, WF ratio, PF, and the dimensionless thermoelectric figure of merit of our device when the quantum dot is connected to monoatomic *sp* or SSH chains, and to diatomic *sp* or RM chains, respectively. Notice that the figure of merit measures the usefulness of the device to produce electrical power. In section 11, we present the high temperature results and finally, we conclude with a discussion of our results and the perspectives of our approach.

1 The Rice-Mele model

The RM model has been used to describe polymeric chains with alternating bonds [87]. It is generally associated with fractional charges that arise due to their topological properties and it is used here to model diatomic *sp*-chains.

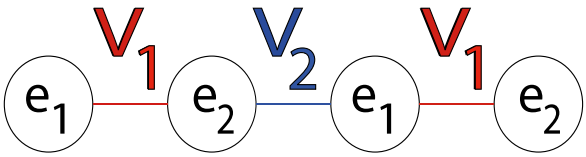

Figure 2.1: Rice-Mele chain

Its Hamiltonian is given by

$$\mathcal{H}_{RM} = -V_1 \sum_n c^\dagger_{A,n} c_{B,n} - V_2 \sum_n c^\dagger_{A,n+1} c_{B,n} + \tag{2.1}$$
$$(e_1 - \mu) \sum_n c^\dagger_{A,n} c_{A,n} + (e_2 - \mu) \sum_n c^\dagger_{B,n} c_{B,n} + H.c.,$$

where $c^\dagger_{(A,B),n}$ and $c_{(A,B),n}$ create and annihilate electrons on site n of sub-lattice (A,B), respectively. The hopping V_1 connect electrons in the same unit cell n, and V_2 those in different unit cells. The site energies $e_{(1,2)}$ are different in sub-lattices A and B and μ is the chemical potential. For a semi-infinite chain the sum extends from $n = 0$ to $n = \infty$. The SSH model is obtained from the RM model, Eq. 2.1, when the site energies are taken equal zero, i.e., $e_1 = e_2 = 0$.

in the notation of Bogoliubov de Gennes

$$\mathcal{H} = \begin{pmatrix} c_{A,k} & c_{B,k} \end{pmatrix} \begin{pmatrix} e_1 - \mu & -V_1 - V_2 e^{ik} \\ -V_1 - V_2 e^{-ik} & e_2 - \mu \end{pmatrix} \begin{pmatrix} c^\dagger_{A,k} \\ c^\dagger_{B,k} \end{pmatrix} \tag{2.2}$$

we then calculate the energies

$$\varepsilon = det((H) - \varepsilon) = 0, \tag{2.3}$$

The energy of the bands of the infinite, translation invariant RM chain can be obtained transforming to momentum space and diagonalizing the Hamiltonian [76]. They are given by

$$\tilde{\omega}_1(k) = -\tilde{\mu} + \sqrt{2\tilde{V}\cos(k) + \tilde{V}^2 + \tilde{\epsilon}^2 + 1} \tag{2.4}$$

$$\tilde{\omega}_2(k) = -\tilde{\mu} - \sqrt{2\tilde{V}\cos(k) + \tilde{V}^2 + \tilde{\epsilon}^2 + 1}. \tag{2.5}$$

The extrema of the bands occur for $k = \pi$. Notice that there is always a gap between the bands, which is given by

$$\tilde{\Delta} = |\tilde{\omega}_1(\pi) - \tilde{\omega}_2(\pi)| = 2\sqrt{(1 - \tilde{V})^2 + \tilde{\epsilon}^2}. \tag{2.6}$$

The *tilde* quantities are dimensionless, normalized by the hopping V_2 and $\tilde{V} = V_1/V_2$. We took $e_1 = -e_2 = \epsilon$. In the case of the SSH model, with $\epsilon = 0$, the band gap closes for $\tilde{V} = 1$, at the topological transition.

The topological properties of the RM and SSH chains are well known [70,76]. For the latter there is a non-trivial topological phase for $\tilde{V} < 1$ characterized by a non-trivial winding number. For $\tilde{V} = 1$ there is a topological transition for a topologically trivial phase with $\tilde{V} > 1$. In the non-trivial topological phase there are edge modes at the ends of a finite chain. These edge states decay into the bulk with a characteristic length that depends on the distance to the topological transition, $\xi = (1 - \tilde{V})^{-\nu}$. At the topological transition ξ diverges and the *surface state* spreads into the bulk [78]. For the SSH model the critical exponent $\nu = 1$.

The topological properties of the RM model are more complex, but also well known [70, 76]. The topological phases can be characterized by Chern numbers [70,76,88,91,92], $n_C = -\text{sgn}[\epsilon(V_2 - V_1)]$, such that for $V_1 = V_2$ or $\epsilon = 0$ there are topological quantum phase transitions [76, 91, 92]. The phase with $\tilde{V} < 1$ is topologically non-trivial. In this work we calculate the winding number

$$W = \frac{-1}{\pi} \int_{-\pi}^{\pi} dk \frac{e^{-ik}}{-\mathcal{S} + 2e^{-ik}}$$

where $\mathcal{S} = \frac{-\varepsilon}{h}$. When $|\mathcal{S}| > 2 \Rightarrow W = 0$ the system is in the trivial phase, if $|\mathcal{S}| < 2 \Rightarrow W = 1$ the system is in the topological phase and if $|\mathcal{S}| = 2$ W is not defined because it jumps in the phase transition.

$$H(k) = - \begin{pmatrix} 0 & h^*(k) \\ h(k) & 0 \end{pmatrix},$$

where $h(k) = V_1 + V_2 e^{ik}$.

We studied too the topological phases of the SSH chain using the winding number obtained in appendix C which is defined by the equation

$$W = 1/2\pi \int_{-\pi}^{\pi} dk \frac{e^{-ik}}{e^{-ik} - \mathcal{S}},$$

where $\mathcal{S} = \frac{-V_1}{V_2}$. When $|\mathcal{S}| > 1 \Rightarrow W = 0$ the system is in the trivial phase, if $|\mathcal{S}| < 1 \Rightarrow W = 1$ the system is in the topological phase and if $|\mathcal{S}| = 1$, W is not defined because it jumps in the phase transition.

In order to obtain the thermoelectric properties of our device, we need to calculate the surface density of states of the semi-infinite RM and SSH chains. Here, we use a method developed in Ref. [89] that yields the local Green's functions at the edge of this chain. This Green's function is obtained from the self-consistent equation,

$$G_{00}(\omega) = \begin{pmatrix} \omega + \mu - \epsilon & V_1 & 0 \\ V_1 & \omega + \mu + \epsilon & V_2 \\ 0 & V_2 & G_{00}^{-1} \end{pmatrix}^{-1}_{(00)}, \tag{2.7}$$

from which, we can get the surface density of states,

$$\rho(\omega) = \frac{-1}{\pi} \mathrm{Im} G_{00}(\omega). \tag{2.8}$$

The surface density of states of the semi-infinite RM chain, obtained from Eqs. 2.7 and 2.8 is given by

$$\rho(\omega) = (D + |D|)\, \delta(\omega + \mu - \epsilon) + \frac{\mathrm{sgn}(\omega + \mu)\, \mathrm{Im}\, m[R(\omega)]}{2(\omega + \mu - \epsilon)} \tag{2.9}$$

where $D = (1 - \tilde{V}^2)$. Notice that for D<0, i.e. in the trivial topological phase with $V_1 > V_2$, the weight of the delta fuction vanishes, since $(D + |D|) = 0$ and there is no surface state in this phase. On the other hand for $V_1 < V_2$, i.e. in the topological phase with D>0, the surface states has a weight giver by 2D. Notice that D vanishes exactly ate the topological transition $V_1 = V_2$ where D=0. With

$$R(\omega) = \left(-(\mu + \omega)^2 + (1 - \tilde{V})^2 + \epsilon^2\right)^{\frac{1}{2}} \times \left(-(\mu + \omega)^2 + (1 + \tilde{V})^2 + \epsilon^2\right)^{\frac{1}{2}} \tag{2.10}$$

Notice the presence of a surface mode at a finite energy $\omega_S = \epsilon - \mu$, for $\tilde{V} < 1$ (since $V_2 = 1$ we keep the *tilde* only in $\tilde{V}$). Differently from the SSH model the RM system is always gapped even at $\tilde{V} = 1$. However, the phases with $\tilde{V} > 1$ and $\tilde{V} < 1$ can still be distinguished by the absence or presence, respectively of the surface mode (besides their Chern numbers) [70, 76, 88, 91, 92]. The phase with $\tilde{V} < 1$ is the topologically non-trivial.

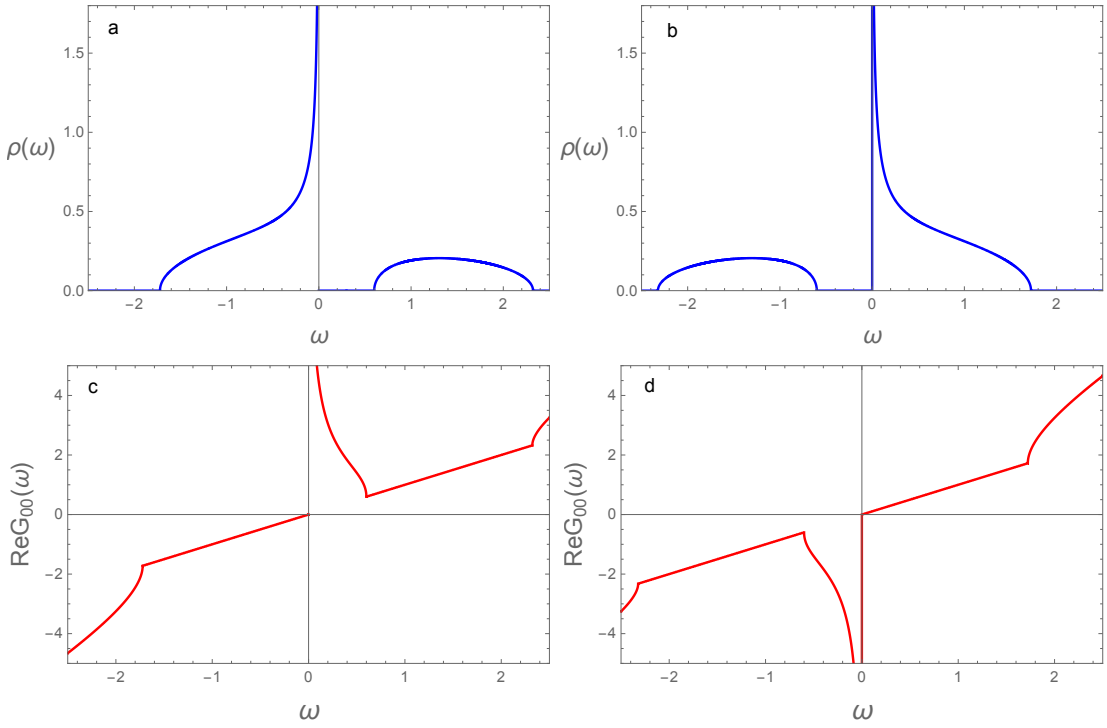

Figure 2.2: (Color online) Surface density of states of the semi-infinite diatomic sp-chain (RM chain), Eq. 2.9, at the topological transition ($\tilde{V} = 1$), for a) $\mu = \epsilon = -0.3$ b) $\mu = \epsilon = 0.3$. Real part of the surface Green's function for c) $\mu = \epsilon = -0.3$ and d) $\mu = \epsilon = 0.3$.

Fig 2.2 shows the surface density of states and the real part of the surface Green's function for RM-chains at the topological transition $\tilde{V} = 1$. The figures are for two values of the energy of the local surface mode, $\epsilon = \pm 0.1$.

The chemical potential is located on the energies of these modes ($\mu = \epsilon$).

2 SSH chains

Let us start with the simpler case of the semi-infinite SSH chain, which corresponds to the RM model with $\epsilon = 0$. the chain studied by Su-Schrieffer-Heeger or better known as the SSH chain it is a linear chain composed of polyenes that have alternate single and double bonds [93] as we can see in the figure 2.3.

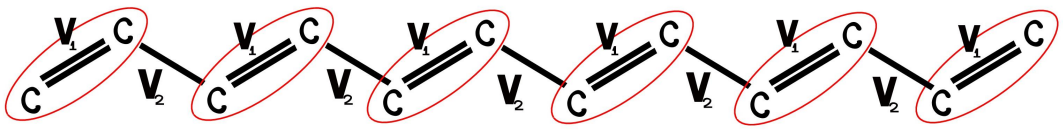

Figure 2.3: SSH chain composed of polyenes, where each red ellipse represents a unit cell

The Hamiltonian of this model is given by:

$$\mathcal{H}_{SSH} = -V_1 \sum_n (a^\dagger_{n,2} a_{n,1} + a^\dagger_{n,1} a_{n,2}) - V_2 \sum_n (a^\dagger_{n+1,1} a_{n,2} + a^\dagger_{n,2} a_{n+1,1}), \tag{2.11}$$

where V_1 and V_2 are alternating hopping terms as in the figure 2.3. This model is equivalent to an SP chain with intra-site interactions [89] where V_1 and V_2 are in this case intra- and inter-cell hybridization terms respectively.

With the Hamiltonian of the SSH chain we take the Fourier transform:

$$\mathcal{H}_{SSH} = -V_1 \sum_k (a^\dagger_{k,2} a_{k,1} + a^\dagger_{k,1} a_{k,2}) - V_2 \sum_k (e^{-ik} a^\dagger_{k,1} a_{k,2} + e^{ik} a^\dagger_{k,2} a_{k,1}),$$

From Eq. 2.7, with $\epsilon = 0$, we obtain a self-consistent problem involving a second degree algebraic equation for the local Green's function,

$$[V_2 G_{00}]^2 - 2\alpha [V_2 G_{00}] + 1 = 0, \tag{2.12}$$

with

$$\alpha(\omega) = \frac{\omega^2 + V_2^2 - V_1^2}{2V_2\omega}. \tag{2.13}$$

We consider the case of half-filled band and take $\mu = 0$. The surface Green's function can be directly obtained from Eq. 2.12. It is given by,

$$G_{00}(\omega) = \frac{1}{2}\frac{1}{\omega}\left[\tilde{\omega}^2 - \tilde{V}^2 + 1 \pm \sqrt{(\tilde{\omega}^2 - \tilde{V}^2 + 1)^2 - 4\tilde{\omega}^2}\right] \tag{2.14}$$

where $\tilde{\omega} = \omega/V_2$, and $\tilde{V} = V_1/V_2$. The surface density of states is obtained from Eqs. 2.8 and 2.14 and is given by

$$\rho(\omega) = \frac{1}{2}\left\{\Big(D + |D|\Big)\delta(\tilde{\omega}) + \frac{1}{\pi}\mathrm{Im}[\frac{\sqrt{(\tilde{\omega}^2 + D)^2 - 4\tilde{\omega}^2}}{\tilde{\omega}}]\right\}. \tag{2.15}$$

where $D = 1 - \tilde{V}^2$ and $\tilde{\omega} \to \tilde{\omega} + i\epsilon$. The sign of the root is chosen so that the density of states is positive and from now on we take $V_2 = 1$. There is an additional contribution to the zero energy mode due to the second, square root term. Considering this explicitly, we can rewrite

Then, we find that the surface Green's function gives direct information on the topological state of the chain. Furthermore, the weight of the zero energy mode vanishes linearly with the distance to the topological transition ($D \propto (1 - \tilde{V})$).

3 Central Charge and Thermalization in the Rice-Mele Model

The Rice-Mele (RM) model constitutes a fundamental paradigm in the study of one-dimensional systems with broken time-reversal symmetry and topology [87]. While its topological phases and charge pumping properties are well-established, a deeper layer of its physics emerges in the context of Conformal Field Theory (CFT) and the thermodynamics of out-of-equilibrium quantum systems. This chapter is dedicated to exploring the properties of the **central charge** in the Rice-Mele model, particularly in the

critical regime where the system exhibits conformal symmetry, and to elucidating the profound connection between this central charge, the entanglement entropy, and the thermal conductance–a relationship supported by general results from the physics of integrable systems and conformal hydrodynamics.

3.1 The Rice-Mele Model and its Conformal Regime

The Rice-Mele model is described by the Hamiltonian [87]:

$$\hat{H} = -\sum_j \left[(t + \delta(-1)^j)(\hat{c}^\dagger_{j+1}\hat{c}_j + \text{h.c.}) + \Delta(-1)^j \hat{c}^\dagger_j \hat{c}_j \right] \tag{2.16}$$

where t is the average hopping, δ breaks the dimerization (Su-Schrieffer-Heeger phase), and Δ is an alternating on-site potential that breaks inversion symmetry.

In its parameter space, there exist critical points where the spectrum becomes gapless and the long-range fluctuations are governed by a CFT. In this regime, the low-energy physics of the model is described by a massive Dirac CFT or, at specific points, by minimal conformal theories [94]. The universal invariant characterizing a CFT is the **central charge** c, which emerges from the renormalization group flow of the model and classifies the conformal theory [95].

4 The Central Charge as a Universal Invariant

The central charge c is a real number that quantifies the anomalous degrees of freedom of the Virasoro algebra in CFT, following the seminal construction by Belavin, Polyakov, and Zamolodchikov [95]. It universally classifies the theory and determines thermodynamic and correlation properties. Its most directly measurable consequence in many-body systems is the behavior of the von Neumann **Entanglement Entropy**.

For a subsystem of length L embedded in a ring of size N (with $N \to \infty$), the entanglement entropy scales as [96]:

$$S(L) = \frac{c}{3} \ln \left[\frac{N}{\pi} \sin \left(\frac{\pi L}{N} \right) \right] + \kappa \tag{2.17}$$

where κ is a non-universal constant. This relation, derived by Calabrese and Cardy, is the primary practical tool for extracting the central charge c from condensed matter systems via numerical methods like DMRG [97]. In the Rice-Mele model, upon approaching a quantum phase transition, the value of c changes, reflecting the change in the effective conformal theory, often to a Dirac fermion with $c = 1$ [94,98].

4.1 The Entropy-Thermal Conductance Relation and the Central Charge

The connection between central charge and energy transport is a cornerstone of conformal hydrodynamics. In a one-dimensional conformal system, the thermal conductance κ is quantized and directly related to the central charge, a result established in the context of the Luttinger liquid formalism [99] and formalized in a general context by authors such as Tomazelli and Di Lorenzo [100].

The thermal conductance of a clean, one-dimensional quantum system coupled to thermal baths is given in the ballistic regime by [101, 102]:

$$\kappa = \frac{\pi k_B^2 T}{6\hbar} c \tag{2.18}$$

where T is the temperature, k_B is Boltzmann's constant, and $\hbar$ is the reduced Planck constant. This formula, analogous to the quantization of electrical conductance in quantum channels, arises from the calculation of the energy-momentum tensor in a conformal theory on a finite segment connected to reservoirs.

This relation establishes a direct and verifiable bridge between:

1. **A quantum information property (Entropy S):** The entanglement entropy, which measures quantum correlations, scales with c [96].

2. **A thermodynamic transport property (Conductance κ):** The system's ability to transport energy is proportional to c [101].

Therefore, in the conformal regime of the Rice-Mele model, the central charge c emerges as the unifying quantity. Measuring the logarithmic growth of the entanglement entropy provides a direct prediction for the quantized value of the system's ballistic thermal conductance, linking two seemingly distinct phenomena under a single universal law.

In summary, the Rice-Mele model, when analyzed through the lens of conformal physics, reveals a rich universal structure governed by its central charge. This quantity, whose origin traces back to the classification of conformal theories [95], is a measurable physical signature that connects the realm of quantum information (through entanglement entropy [96, 97]) to the realm of out-of-equilibrium thermodynamics (through quantized thermal conductance [101, 102]). The relation $\kappa \propto c$ consolidates the understanding that ballistic energy transport in one-dimensional systems is a universal phenomenon, dictated by the underlying conformal symmetries. The study of the Rice-Mele model in this context therefore serves as a prototype for understanding thermalization and transport in a wide range of one-dimensional materials, from spin chains to quantum wires.

5 Thermoelectric properties of two semi-infinite chains coupled to a quantum dot

In this section we study the transport properties of a device consisting of two identical semi-infinite chains connected to a quantum dot [90, 103], as shown in Fig. 2.4. Since we are dealing with spinless fermions, the dot can either be empty, or singly occupied. The non-interacting quantum dot has a single state with energy E_0 and is coupled to the chains by a hopping term t_d that transfers quasi-particles in and out of the dot. Then, the dot provides a connection between the semi-infinite chains and allows to probe the nature of the edge states through their contribution to the thermal and electrical conductances of the device, as we discuss below. The coupling Hamiltonian between the dot and the

semi-infinite chains is given by, $H_c = -\sum_\alpha t_{d,\alpha} c^+_{\alpha,0} d + H.c.$, where the second quantization operators c and d refer to the chains and dot and $\alpha = r, l$ to the right and left chains, respectively. The dot couples to the first site of each chain (site 0) [104]. For simplicity, we take here $t_{d,r} = t_{d,l} = V$. The full local Green's function of the dot connected to the two semi-infinite chains is given by [104],

$$G_d(\omega) = \frac{g_d}{1 - 2|V|^2 g_d G_{00}} \tag{2.19}$$

where,

$$g_d = \frac{1}{\omega - E_0} \tag{2.20}$$

is the Green's function of the non-interacting dot. The Green's function G_{00} is that of the edge of the chains and is given by the self-consistent solution of Eq. 2.7. Notice that Eq. 2.19 can be rewritten as,

$$G_d(\omega) = \frac{1}{\omega - E_0 - 2|V|^2 \mathrm{Re}G_{00} - i2|V|^2 \mathrm{Im}G_{00}}. \tag{2.21}$$

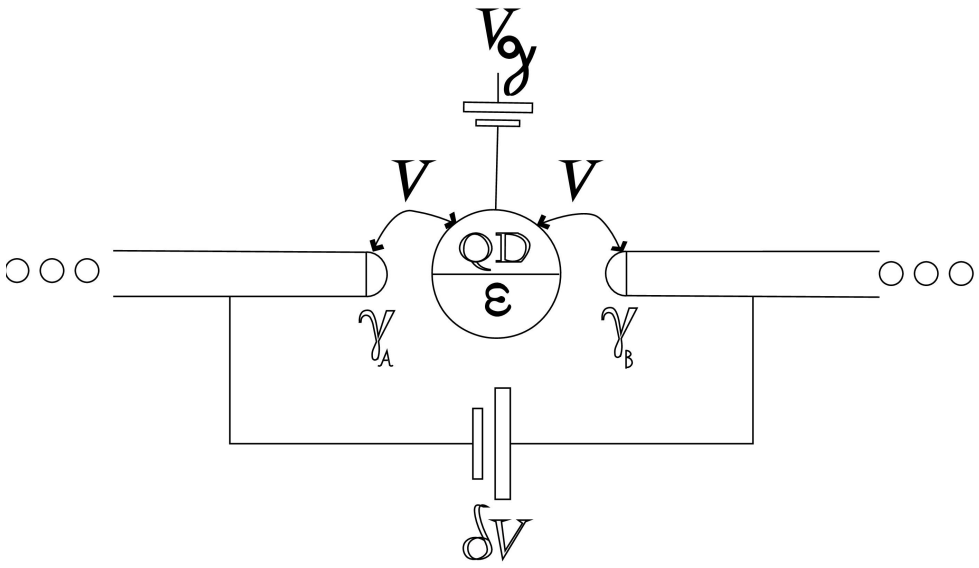

Figure 2.4: Two semi-infinite *sp*-chains connected to a QD. A very small potential difference δV is applied in the chains. Notice that V is the coupling between the dot and the chains and V_g is the gate potential that controls the energy level of the QD.

The dimensionless electrical conductance of the device, *chain-dot-chain* can be obtained as in Ref. [105]. It is given by,

$$\mathcal{L}_n = \frac{1}{h} \int d\omega (-\frac{\partial f}{\partial \omega}) \omega^n \mathcal{T}(\omega), \tag{2.22}$$

in terms of which we can obtain the thermoelectric coefficients. The conductance can be rewritten as $G = e^2 \mathcal{L}_0$. The thermal conductance K and the thermopower S are given, respectively, by

$$K = \frac{1}{T} \left(\mathcal{L}_2 - \frac{\mathcal{L}_1^2}{\mathcal{L}_0} \right), \tag{2.23}$$

$$S = -\left(\frac{1}{eT}\right)\frac{\mathcal{L}_1}{\mathcal{L}_0}. \tag{2.24}$$

These in turn define the WF ratio and the dimensionless *figure of merit* ZT that are given, respectively, by

$$WF = \frac{1}{T}\left(\frac{K}{G}\right), \tag{2.25}$$

$$ZT = \frac{S^2 GT}{K}, \tag{2.26}$$

where the former ratio WF is given in units of the Lorenz number $L_0 = (\pi^2/3)(k_B/e)^2$. The Mahan-Sofo parameter ζ [106] is defined in terms of the thermoelectric coefficients

$$\zeta = \frac{L_1^2(T)}{L_0(T)L_2(T)}, \tag{2.27}$$

and using this parameter, the dimensionless thermoelectric figure of merit, defined in Eq. (2.26), can be written as

$$ZT = \frac{\zeta}{1-\zeta}. \tag{2.28}$$

The best ZT occurs at the limit $\zeta \to 1$.

6 Results for SSH chains or monoatomic sp-chains

We start obtaining the thermoelectric properties of the device in the case the dot is coupled to SSH chains. We calculate, using the equations above, the thermoelectric properties of the coupled system, dot-chains, in the different topological phases of the SSH chains and at the topological transition. When the chains are in either the trivial or topological phases, i.e., for $\tilde{V} > 1$ and $\tilde{V} < 1$, respectively, the conductances are zero at zero temperature, since the bulk of the chains are insulators. At finite temperatures these conductances become finite due to thermal activation of quasi-particles above the band gap. The results presented are obtained for the chemical potential of the chains $\mu = 0$, i.e., for a full lower band (*half-filling*). The dot energy is $E_0 = 0$, and the coupling between the dot and the chains is taken as, $t_d/V_2 = 0.15$. Fig. 2.5a shows the conductance of the device in the trivial and topological phases. As expected the conductances vanish at $T = 0$ in both phases and become finite at finite temperatures. The finite temperature conductance is larger in the topological phase. Notice that in both cases shown, $\tilde{V} = 1.03$ and $\tilde{V} = 0.97$, the system is at the same distance of the topological transition at $\tilde{V} = 1$. The increment of the conductance in the topological phase can be attributed to the presence of the edge mode.

Fig. 2.5b shows the thermal conductivity divided by temperature, in units of $G_0 L_0$. They also vanish for $T = 0$, in both the trivial and topological phases, as expected, since the *bulk* of the chains is insulating.

Fig. 2.5c shows the WF ratio, defined as $WF = (K/T)/(G/G_0)$ and in units of $G_0 L_0$, as a function of temperature. Away from the topological transition in both trivial and topological phases the WF law is violated. This can occur in topological systems [71,107], as for the monoatomic chains and in general for diatomic chains, as we discuss below and show in Fig. 2.12.

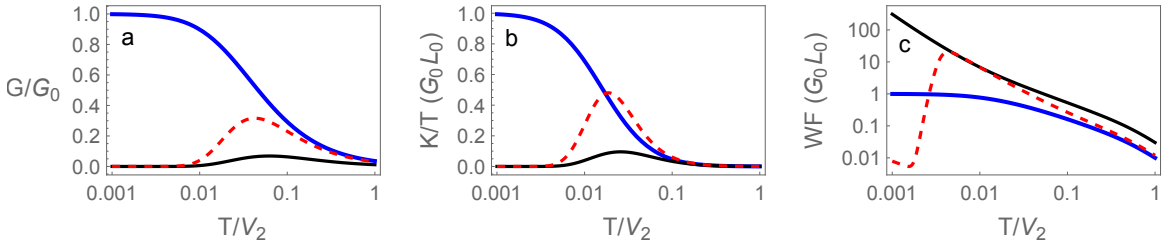

Figure 2.5: (Color online) a) Dimensionless electrical conductance, b) thermal conductivity divided by temperature in units of G_0L_0 and c) WF ratio ($WF = (K/T)/(G/G_0)$) in units of G_0L_0 as functions of temperature for the device with SSH chains. In the trivial phase ($\tilde{V} = 1.03$) black continuous, topological phase ($\tilde{V} = 0.97$) red dashed and at the topological transition ($\tilde{V} = 1$) blue continuous.

Fig. 2.5a, b and c, also show the conductance, thermal conductivity and WF ratio *at the topological transition*, i.e., at $\tilde{V} = 1$. The zero temperature dimensionless electrical conductance in this case is unity showing that a quantum of charge flows through the system. Then, at the transition the surface modes recombine to form a quasi-particle that transports electric current through the dot. The current can flow through the device since, at $V_1 = 1$, the chains are in a semi-metallic state (Dirac semi-metal). We point out that the zero temperature electrical conductance at the transition does not depend on the coupling t_d between the dot and the chains. The thermal conductance K, differently from the electrical conductance vanishes at zero temperature, even at the topological transition. However, the temperature normalized thermal conductance (K/T) at the topological transition goes in this limit to 1, in units of G_0L_0 , as shown in Fig. 2.5 b. The WF ratio, at the topological transition of the monoatomic chain, starts as unity at $T = 0$ and remains constant at very low temperatures showing that the WF law is obeyed in this case. Finally, we remark that the thermopower, Eq. 2.24, vanishes at the trivial and topological phases and also at the topological transition. This occurs since the quantity $\mathcal{L}_1$ in this equation cancels out due to equal but opposite contributions of electrons and holes to this quantity in this particle-hole symmetric case.

7 Results of the diatomic *sp* or Rice-Mele chains

In this section we obtain the thermoelectric properties of the device when RM chains are attached to the QD. Notice that in this case the chiral symmetry of the SSH chain is broken for RM chains. We consider the situation where the chemical potential coincides with the local energy of one of the sub-lattices, i.e., we take $\mu = \pm\epsilon$. Furthermore we consider that the quantum dot is in resonance with the energy of the edge mode, which for the condition $\mu = \pm\epsilon$ corresponds to take $E_0 = 0$. Since $\epsilon \neq 0$, the topological transition of the model occurs for $\tilde{V} = 1$. We start showing the normalized temperature dependent conductances of the RM model at the topological transition. As can be seen in Fig. 2.6, the normalized conductances at zero temperature now attains a value of $1/2$, expected when fractional charges

$e/2$ are responsible for the electronic transport in the system. This result is universal in the sense that it is independent of the coupling t_d between the dot and the chains and the value of ϵ, for the conditions specified above ($\mu = \pm\epsilon$, $E_0 = 0$). Whenever we use this term here we refer to this type of universality. The figure shows the normalized conductance for two values of ϵ/V_2. Notice that for $\epsilon/V_2 \ll 1$ the finite temperature conductance reaches a maximum value close to one, as if there is a recombination of the fractional charges in the system due to thermal effects.

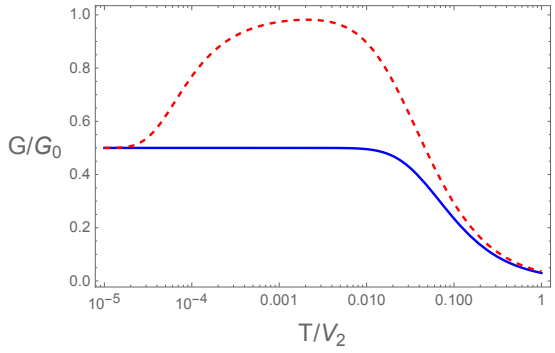

Figure 2.6: (Color online) Normalized conductances as a function of temperature for a system consisting of two semi-infinite RM chains attached to a quantum dot at the topological phase transition of the chains ($\tilde{V} = 1$). In blue continuous $\epsilon/V_2 = 0.1$, and in red dashed $\epsilon/V_2 = 5 \times 10^{-5}$. In both cases, the low temperature saturation value $G/G_0 = 1/2$ gives evidence of fractional charges flowing in the system. The curves for G/G_0 are independent of the coupling to the QD and of the sign of ϵ, for $\mu = \epsilon$ and the dot in resonance with the edge mode. Notice that for small values of ϵ/V_2 as temperatures increases there is a kind of recombination of the fractional charges.

We point out that the fractional charge as evidenced by the zero temperature conductance is a direct consequence of the breaking of chiral symmetry of the original SSH model, due to the finite and distinct energies of the sub-lattices of the RM model.

8 Thermopower

The thermopower is an interesting and unique physical property that contains fundamental information on both, transport and thermodynamic properties of the system. The temperature dependence of the thermopower of the device consisting of two RM chains coupled to the quantum dot can be obtained using Eq. 2.24. At the topological transition ($\tilde{V} = 1$), this is shown in Fig. 2.7 for $\mu = \epsilon$ and the cases of ϵ positive and negative. The corresponding surface density of states for these two cases is shown in the upper panels of Fig. 2.2. The thermopower is positive or negative depending whether the charge carriers are holes or electrons, respectively. It is constant at low temperatures and its absolute value decreases with increasing temperature. It is remarkable that it does not vanish for $T \to 0$, as expected from the third law of thermodynamics. Mathematically, this arises since the function $\mathcal{T}(\omega)$ in Eq. 2.22 has a jump

discontinuity and is non-differentiable at $\omega = 0$, which precludes a low temperature Sommerfeld expansion. The constant low temperature values for the thermopower, $S(T \to 0) \approx \pm 1.386$ can be rationalized in terms of the properties of the quantum dot and of the chains at the topological transition. Since we took $\mu = \epsilon$, the doubly degenerate zero energy surface mode [108] becomes delocalized at the transition and every site in the system including the dot has a double degenerescence. For a system of charged particles, the thermopower represents the entropy per carrier divided by the charge of the carrier [109],

$$S_0 = \frac{\text{entropy per carrier}}{q^*}. \tag{2.29}$$

This is also known as the Kelvin formula for the Seebeck coefficient [110]. The entropy per site is $S = \ln 2$ and remains finite at $T = 0$ due to the double degeneracy of the states, whether a site is occupied by a particle or by a hole. If the carriers have a fractional charge, $q^* = \pm 1/2$ (in units of electric charge) as evidenced by the zero temperature conductance, we get

$$S_0 = \frac{\ln 2}{(\pm 1/2)} = \pm 2 \ln 2 \approx \pm 1.386 (k_B/e), \tag{2.30}$$

which are exactly the low temperature saturation values, obtained numerically for the thermopower using Eq. 2.24, as shown in Fig. 2.7. These values are universal in the same sense we used for the conductance, i.e., they are independent of ϵ and t_d (for $\mu = \epsilon$, $E_0 = 0$).

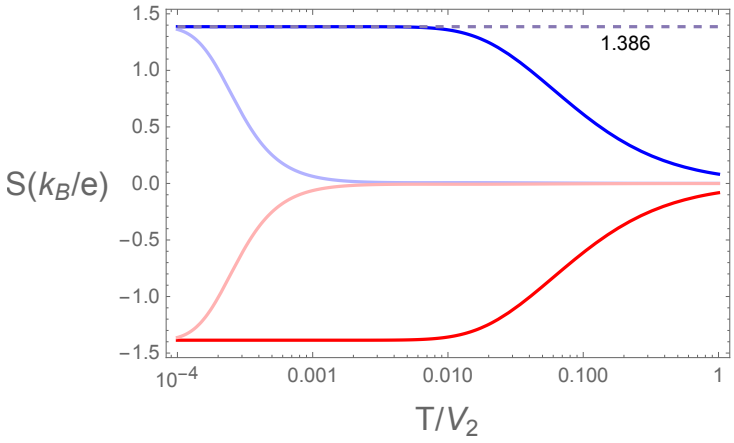

Figure 2.7: (Color online) Thermopower of the device as a function of temperature in units of (k_B/e) at the topological transition of the RM chains. $S > 0$ correspond to $\mu = \epsilon = +0.1$, and $\mu = \epsilon = +3.3 \times 10^{-4}$ (light curve). Negative thermopower ($S < 0$) corresponds to $\mu = \epsilon = -0.1$ and $\mu = \epsilon = -3.3 \times 10^{-4}$ (light curve). The light color curves show the trend to the results the SSH chain with $\epsilon = 0$. The energy scale for the low temperature saturation of the thermopower is given by the difference in site energies, 2ϵ. The numerical results for the saturation values, $S(T = 0) \approx \pm 1.38634$ are in close agreement with $S_0 = \pm 2 \ln 2 \approx \pm 1.38634$, as discussed in the text.

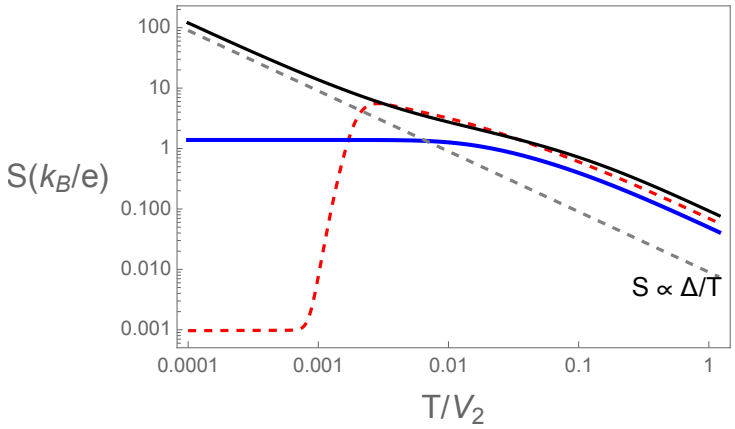

Figure 2.8: (Color online) Thermopower of the device as a function of temperature in units of (k_B/e) away and at the topological transition of the RM chains. Red dashed corresponds to $\tilde{V} = 0.95$, such that the chains are in the topological phase. Black continuous shows the thermopower in the trivial phase, with $\tilde{V} = 1.05$ and blue at the topological transition. The gray dashed line shows the classical result for a semiconductor with activation energy Δ.

Then this result for the thermopower, together with that for the electrical conductance, corroborate the existence of carriers with fractional charges, $q = \pm e/2$, flowing in the device with RM chains at the topological transition. This *transport charge* does not necessarily coincide with the notion of a *boundary charge* in topological chains [111]. This concept is useful when the system is in the non-trivial topological phase but away from the topological transition [111]. The wave function of the edge modes is finite inside the bulk of the material, and the boundary charge is obtained by integrating over a finite characteristic length that depends on the model's parameters. The fractional charges we get from the transport properties appear at the topological transition. In this case, the relevant length scale is the penetration depth of the edge modes that diverge at this transition [78, 112, 113]. It implies that the edge mode charge is spread all over the system; consequently, the concept of a boundary charge becomes meaningless. For completeness we show in Fig. 2.8 the temperature dependent thermopower away from the topological transition in both trivial and non-trivial topological phases.

9 Thermal conductance and Wiedemann-Franz ratio

The thermal conductance divided by temperature (K/T) at the topological transition of the diatomic *sp*-chain is shown in Fig. 2.10. From Eqs. 2.22 to 2.25, we can write

$$\frac{K}{T} = \frac{\mathcal{L}_2}{T^2} - \left(\frac{\mathcal{L}_1}{eT\mathcal{L}_0}\right)^2 e^2\mathcal{L}_0, \tag{2.31}$$

and using the expressions for the thermopower and conductance we get,

$$\frac{K}{T} = \frac{\mathcal{L}_2}{T^2} - S^2 G. \tag{2.32}$$

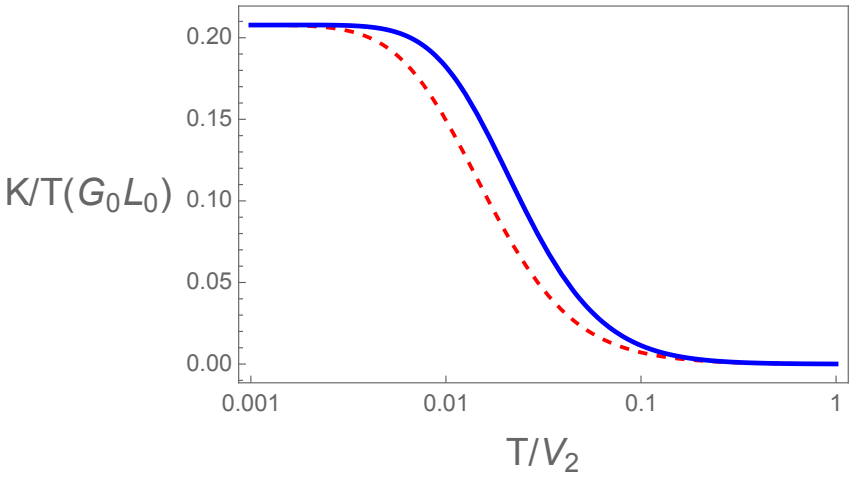

Figure 2.9: (Color online) Thermal conductance divided by temperature of the device at the topological transition of the RM chains in units of G_0L_0, where L_0 is the Lorenz number for $\epsilon = 01$ blue continuous, and $\epsilon = 0.3$ red dashed. The zero temperature limiting value $(K/T)_0 \approx 0.20792$ (see text). is independent of the values of t_d and ϵ as long as, $\mu = \epsilon$ and $E_0 = 0$.

We can obtain the limit of zero temperature analytically, $(K/T)_0 = (K/T)_{T\to 0}$, using the results for the thermopower, Eq. 2.30, and for the conductance. We find,

$$(K/T)_0 = \frac{1}{2}(1 - \frac{3}{\pi^2}(2\ln 2)^2) \approx 0.20792, \tag{2.33}$$

in units of G_0L_0. This is in agreement with the numerical result shown in Fig. 2.9 and it is independent of ϵ and t_d. The dimensionless WF ratio attains at zero temperature the value, $\mathcal{W} = (WF/L_0) = 1/2$. This value of $\mathcal{W}$ is different from that for metallic chains where $\mathcal{W} = 1$. Violation of the WF law has been found in interacting systems [71, 114] and in devices with interacting quantum dots [115, 116].

For completeness, we point out that away from the topological transition, both in the trivial and non-trivial topological phases we obtain that the conductance and thermal conductivities are thermally activated as in a semi-conductor.

10 Figure of merit and power factor

Fig. 2.10 shows the dimensionless power factors [106] and figures of merit $ZT = (S^2GT)/K$ of the device, as functions of temperature, at the topological transition, $\tilde{V} = 1$, and in the trivial $\tilde{V} = 1.05$ and topological $\tilde{V} = 0.95$ phases of the RM chains. The power factor is defined as $PF = (\widetilde{PF}/S_0^2G_0)$, where S_0 is the zero temperature thermopower and G_0 the unit of conductance. The quantity $\widetilde{PF} = S^2G$ is the full dimensional power factor [117]. These quantities ZT and PF do not depend on the sign of ϵ, only on its absolute value.

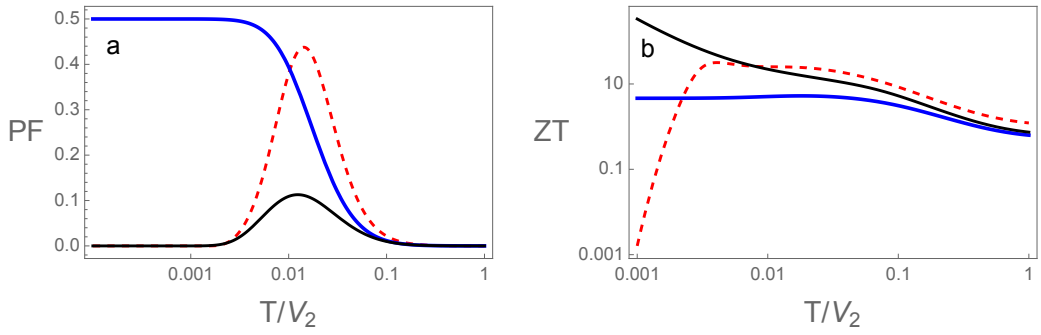

Figure 2.10: (Color online) a) Dimensionless electrical conductance, b) thermal conductivity divided by temperature in units of G_0L_0 and c) WF ratio ($WF = (K/T)/(G/G_0)$) in units of G_0L_0 as functions of temperature for the device with SSH chains. In the trivial phase ($\tilde{V} = 1.03$) black continuous, topological phase ($\tilde{V} = 0.97$) red dashed and at the topological transition ($\tilde{V} = 1$) blue continuous.

Notice that the ZT at the trivial and topological phases assume large values, for the parameters used in Fig. 2.10 at a temperature of$T/V_2 \approx 0.01$, where the power factor is close to a maximum. In order to translate this in physical temperature notice that the energy scale V_2 is of the order of a bandwidth ($\sim$ 1 eV or $\sim 10^4$ K). In the trivial semiconductor phase although the figure merit increases at lower temperatures, the power factor drops to very small values, while it continues significant at the topological transition. The significance of this quantity PF is that, in a time reversible system at steady state, the maximum power for conversion of heat into work is given by $P_{max} = (1/4)\widetilde{PF}$ for two heat reservoirs with a difference in temperature $\Delta T = 1$ K. The efficiency of a device at this maximum power is given by [117],

$$\eta(P_{max}) = \frac{\eta_{ca}}{2}\frac{ZT}{ZT+2} \tag{2.34}$$

where η_{ca} is the efficiency of a Carnot engine working between the same reservoirs. It is worth emphasizing that the relevant characteristic temperatures we obtain, for example, for the saturation of the thermopower at low temperatures, maxima of PF, saturation of WF using reasonable values for the parameters of the dot-chains system are much larger than the actual Kondo temperature of realistic quantum dots [118, 119].

11 High temperature results

In this section we present the results for the thermally activated thermoelectric properties of the device coupled to RM chains.

In Fig.2.11 we present the density of states for different values of the ratio $V_1/V_2 = 1.2; 1.0; 0.8; 0.5$. Two points should be noticed here: First, at the topological phase transition, $V_1/V_2 = 1.0$, the density of states (red curve) presents a sharp behavior at $\mu = 0$ that gives rise to an electrical conductance $G/G_0 = 0.5$ at low temperatures. In contrast, inside the topological region, the density of states at the

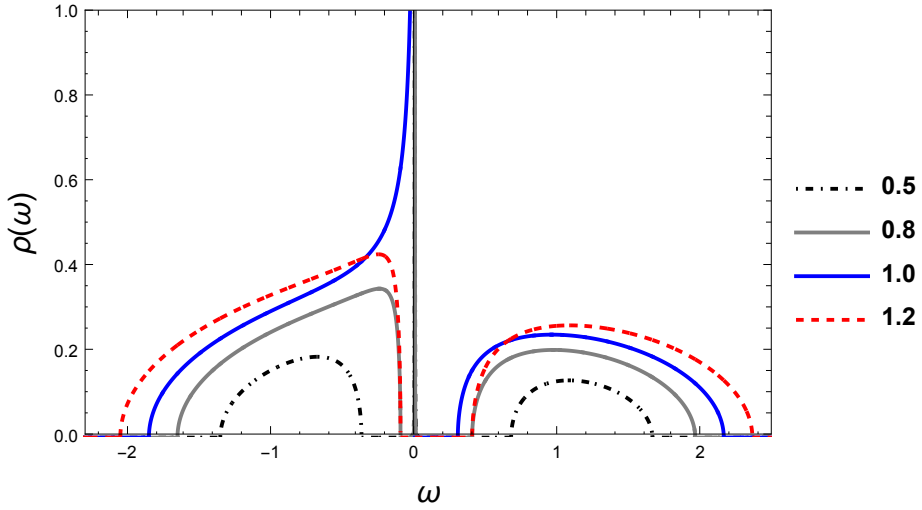

Figure 2.11: (Color online) Density of states corresponding to different values of $V_1/V_2 = 1.2; 1.0; 0.8; 0.5$. The legends represent the values of $\tilde{V} = V_1/V_2$.

chemical potential presents a delta function, as indicated in the curves with $V_1/V_2 = 0.8, 0.5$. On the other hand, the curve $V_1/V_2 = 1.2$, outside the topological region, exhibits a full gap. The second point, and the most important for our purposes, is that inside the topological region, as V_1/V_2 decreases, the electrons migrate from the valence band to the peak located at the chemical potential, increasing its weight and the gap, allowing for tuning the thermoelectric properties to the room temperatures region.

In Figs. 2.12(a,b,c,d) we plot the transport thermoelectric properties for different values of the ratio $V_1/V_2 : a)1.2;\ b)1.0;\ c)0.8;\ d)0.5$. Fig. 2.12(a) shows a high ZT value, but the Power factor is very low, which limits the usefulness of this region. At the topological transition $V_1/V_2 = 1.0$ (Fig. 2.12(b)), ZT, ξ and the PF attain robust values. As V_1/V_2 decreases, the gap increases as indicated in Fig. 2.11; the ZT, ξ and the PF attain high values for $V_1/V_2 = 0.95$ (Fig. 2.12(c)). For $V_1/V_2 = 0.80$, the peak of ZT, ξ and the PF occur at around $T/V_2 = 0.1$ (Fig. 2.12(d)). However, the thermoelectric properties value tends to decrease for low values of V_1/V_2.

Topological insulating chains have many exciting properties. These chains can be realized in materials with hybridized *sp*-states where the anti-symmetric nature of the hybridization between orbitals of different parities guarantees their topological properties. We consider in this Chapter monoatomic and diatomic *sp*-chains that map directly in the SSH and Rice-Mele problems, respectively. We obtain the density of states at the edge of a semi-infinite chain, which varies according to the topological phase of the chain. We show that the weight of the zero energy modes in the non-trivial topological phase vanishes continuously with the distance to the topological transition.

In order to study the transport properties of the chains, we considered a simple device consisting of a QD connected to two identical semi-infinite *sp* or RM chains. Away from the topological transition and at $T = 0$, the current through the device vanishes since the chains are insulators in their bulk, whether they are in the topologically trivial or non-trivial phases. However, at finite temperatures there

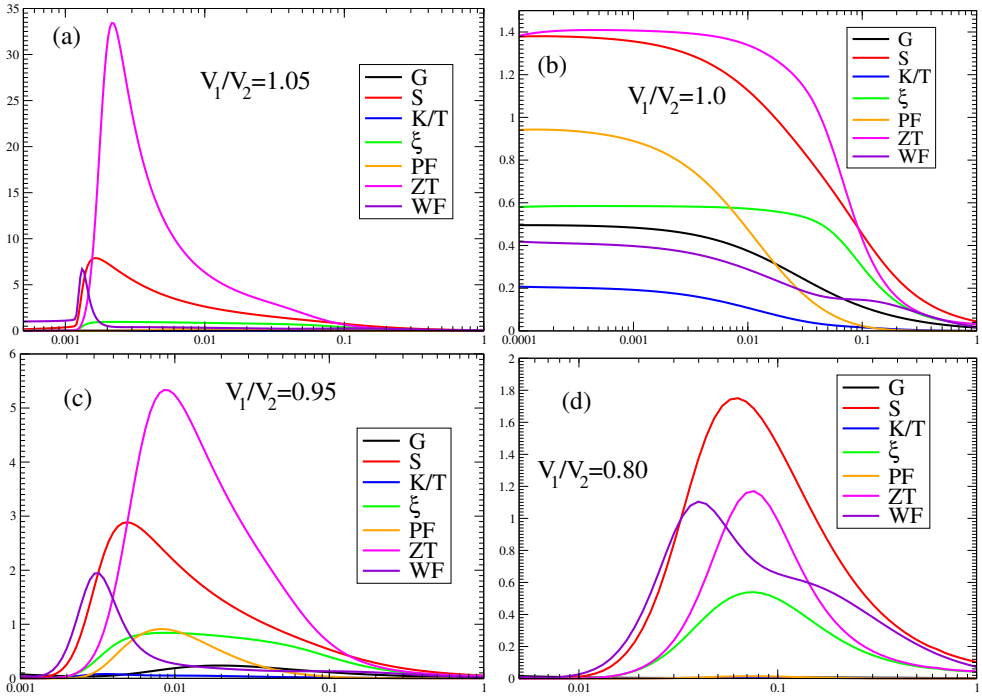

Figure 2.12: (Color online) Temperature activated thermoelectric properties for different values of the hybridization V_1/V_2 : a)1.2; b)1.0; c)0.8; d)0.5.

is activated transport that is different in the trivial and topological phases. This work focuses on the linear response regime or zero voltage limit. It would be interesting to study this same problem at finite voltage. It will be the subject of future research, as it requires an entirely different approach, namely the Keldish formalism [120].

At the topological transition of the monoatomic, or SSH chains, and zero temperature, the conductance in the device has a finite universal value $G/G_0 = 1$, independent of the parameters of the model like the coupling between the chains and the dot, as long as the energy of the dot $E_0 = 0$. Since, at the transition, the surface modes penetrate into the bulk, the system carries current even at $T = 0$. The normalized WF ratio turns out to be equal unity in terms of the Lorenz number. The thermal conductivity vanishes at $T = 0$ even at the topological transition and the thermopower of the monoatomic chains always vanishes due to particle-hole symmetry. A different behavior arises when we consider diatomic *sp*-chains with different sub-lattices local energies. In this case the finite local energies break the chiral symmetry of the SSH Hamiltonian and the chain is now modeled by the RM Hamiltonian. This system still presents non-trivial topological phases that are now characterized by Chern numbers. Interestingly, the zero temperature dimensionless conductance at the topological transition assumes the value $G/G_0 = 1/2$, as would be expected for carriers with a fractional charge and is a consequence of the breakdown of chiral symmetry of the SSH model. The thermopower of the device in this case has an anomalous behavior and does not vanish at low temperatures. It attains a universal value at $T = 0$ consistent with the result for the conductance that implies fractional charges $q^* = 1/2$ flowing in the system. This is due to the double degeneracy of the system associated with the presence of zero

energy modes. it is interesting to compare the physical properties of the fractional charge carriers in the topological insulators with those of Majorana modes in p-wave superconductors [121].

Notice that the antisymmetric hybridization responsible for the non-trivial topological properties of chains does not mix the spins of the carriers. This is quite distinct from the case of spin-orbit interactions that mixes the spins. The consequence is that it is much easier to produce a singly polarized material in the former case. The *sp*-chains, with edge modes in their topological phases are easier to realize in practice than *p*-wave superconductors. Carbyne, the one-dimensional allotropic form of carbon with hybridized *sp* orbitals provides a realization of these chains. They are potentially useful systems exhibiting properties that can be explored in a large temperature range. In particular, we show that varying V_1/V_2, the figure of merit and power factors can attain high values at high temperatures, making the system very attractive to be explored in technological applications.

Chapter 3

Interplay between topology and interactions in superconducting chains

The interest in this chapter is to explore the robustness of topological properties when there are electronic correlations, or disorder, present in materials by presenting a non-trivial topological interaction model with an exact solution for some values of its parameters. As previously stated, the FK model plays an important role in the study of strongly correlated systems, such as heavy fermions and mixed-valence materials. The model consists of a conduction band of itinerant electrons interacting with a background of localized electrons. To do this, it is necessary to define what localized electrons are.

1 Localized electrons

Atoms with a large mass number have electrons in the d and f electron shells that are highly localized close to the nucleus due to the lanthanide contraction effect [122], so that the remaining electrons in the s and p shells are considered practically free, as they move more freely because they are in more external positions of the electron shell, compared to those in the d and f shells. An example of a family that has localized electrons are the rare earths, atoms known as heavy fermions that have an effective mass greater than the mass of a free electron. This behavior occurs due to strong interactions between electrons and can be described by more complex quantum models such as the Kondo, Anderson, Fermi-Liquid models, among others. The lanthanide contraction [122] is characterized by the decrease in the atomic size (atomic radius) of the elements in this series as the atomic number increases from Lanthanum (Z=57) to Lutetium (Z=71), even though the number of electrons in the outer layers (mainly in the 4f sublevel) is almost constant. The second part of the work will focus on the study of the Kitaev chain with FK interaction with localized electrons, thus introducing disorder into the system. The main interest is in defining a condition that results in exact solutions, enabling a detailed analysis regarding the interaction between disorder and the topology of the Kitaev chain, which is already extensively known.

2 The Hamiltonian

The Hamiltonian that describes a chain of spinless fermions, with p-wave pairing, interacting with a background of localized electrons through a FK interaction [21], can be written as a sum of three contributions. The first is the Kitaev one [3, 4],

$$\mathcal{H}_{\mathcal{K}} = -\sum_{i,j} t_{ij} c_i^\dagger c_j - \sum_{i,j} \left(\Delta_{ij} c_i^\dagger c_j^\dagger + \Delta_{ij}^* c_i c_j \right) - \mu \sum_i c_i^\dagger c_i. \tag{3.1}$$

The localized electrons [21] are described by,

$$\mathcal{H}_{\mathcal{L}} = \sum_i (E_f - \mu) f_i^\dagger f_i, \tag{3.2}$$

where in these equations, t_{ij} is the hopping term of the conduction c-electrons, Δ_{ij} the p-wave pairing of electrons in neighboring sites, E_f the energy of the localized f-electrons and μ the chemical potential. Finally, the coupling between the itinerant c-electrons and the localized f-electrons is of the FK type [21] and given by,

$$\mathcal{H}_{\mathcal{FK}} = J \sum_i \left(f_i^\dagger f_i - \frac{1}{2} \right) \left(c_i^\dagger c_i - \frac{1}{2} \right) = J \sum_i \left(n_i^f - \frac{1}{2} \right) \left(n_i^c - \frac{1}{2} \right). \tag{3.3}$$

In order to solve the full Hamiltonian $\mathcal{H} = \mathcal{H}_{\mathcal{K}} + \mathcal{H}_{\mathcal{L}} + \mathcal{H}_{\mathcal{FK}}$, we introduce sets of Majorana operators [123], α_A, α_B, β_A and β_B, such that,

$$\begin{aligned} c_i &= (\alpha_{Bi} + i\alpha_{Ai})/2, \\ c_i^\dagger &= (\alpha_{Bi} - i\alpha_{Ai})/2, \end{aligned} \tag{3.4}$$

where the Majoranas are their own anti-particles, i. e., $\alpha_{A,B}^\dagger = \alpha_{A,B}$. Similarly, for the f-electrons we have,

$$\begin{aligned} f_i &= (\beta_{Bi} + i\beta_{Ai})/2, \\ f_i^\dagger &= (\beta_{Bi} - i\beta_{Ai})/2, \end{aligned} \tag{3.5}$$

where $\beta_{A,B}^\dagger = \beta_{A,B}$. In terms of these new operators we can write the interaction term as,

$$\mathcal{H}_{\mathcal{FK}} = \frac{J}{4} \sum_i (i\beta_{Bi}\beta_{Ai})(i\alpha_{Ai}\alpha_{Bi}). \tag{3.6}$$

For the other terms in the Hamiltonian, we get in the Majorana basis,

$$\mathcal{H}_{\mathcal{K}} + \mathcal{H}_{\mathcal{L}} = -\frac{\mu}{2} \sum_i (1 + \alpha_{Bi}\alpha_{Ai}) - \frac{i}{2} \sum_i \left[(\Delta + t)\alpha_{Bi}\alpha_{Ai+1} + (\Delta - t)\alpha_{Ai}\alpha_{Bi+1} \right] - \frac{\mu - E_f}{2} \sum_i (1 + \beta_{Bi}\beta_{Ai}). \tag{3.7}$$

The many-body problem given by $\mathcal{H} = \mathcal{H}_{\mathcal{K}} + \mathcal{H}_{\mathcal{L}} + \mathcal{H}_{\mathcal{FK}}$ is complex to solve, however a solution can be obtained in some cases.

3 The solution

$$\alpha_{Ai} = \sum_k e^{ikr_i} \alpha_A(k), \tag{3.8}$$

and an equivalent equation for α_{Bi}. Since $\alpha_A^\dagger(k) = \alpha_A(-k)$, only $\alpha_A(k=0)$ is a Majorana operator [123]. In terms of these operators the Hamiltonian can be written as,

$$\mathcal{H} = -\frac{i}{2}\sum_k \left[(\Delta + t)e^{ik}\alpha_B(k)\alpha_A(-k) - (\Delta - t)e^{-ik}\alpha_B(k)\alpha_A(-k)\right] + iJ\sum_k \alpha_A(k)\alpha_B(-(k+Q)), \quad (3.9)$$

where we wrote $J_i = Je^{iQr_i}$. The homogeneous configuration, with a localized electron on each site of the lattice, $n_{fi} = 1$, corresponds to $Q = 0$. The staggered configuration, where the values of K_i alternate between ± 1, such that n_{fi} takes values 0 and 1 in consecutive sites, corresponds to $Q = \pi$. A combination of phases can be used to describe different types of super-lattices [124]. Notice that $n_{fi} = (1/2)(1 + i\beta_{Ai}\beta_{Bi})$. Among all possible configurations, the $Q = 0$ and $Q = \pi$ play an important role, as we discuss below. The excitations of the system are given by the k-dependent eigenvalues of the

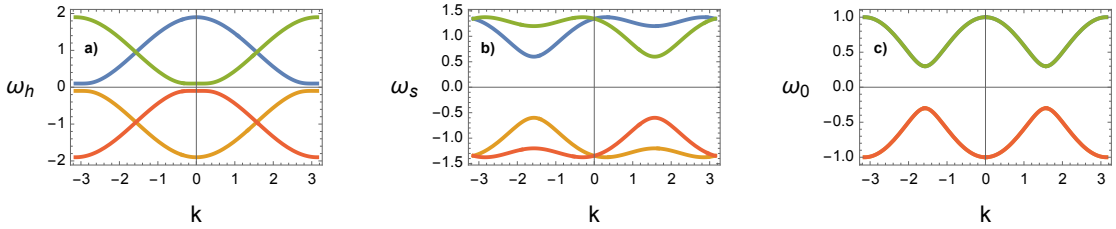

Figure 3.1: (Color online) Dispersion relations of the excitations in the superconducting state with $t = 1$, $\Delta/t = 0.2$ and $J/t = 0.9$. a) homogeneous case ($Q = 0$, $\langle n_f \rangle = 1$), $\omega_h(k)$, and b) staggered case ($Q = \pi$, $\langle n_f \rangle = 1/2$), $\omega_s(k)$. c) energy of the bogoliubons $\omega_0(k)$, of the non-interacting case with the same parameters, but $J = 0$ (Kitaev chain). The conduction band is always half-filled, and $\mu = E_f = 0$.

Hamiltonian Eq. 3.9 [3, 125]. For the homogeneous configuration ($Q = 0$), we get,

$$\omega_{h(1,2)}(k) = \frac{\sqrt{\Delta^2 + 2J^2 \pm 4Jt\cos(k) + \cos(2k)\,(t^2 - \Delta^2) + t^2}}{\sqrt{2}}, \quad (3.10)$$

and $\omega_{h(3,4)}(k) = \pm\omega_{h(1,2)}(k)$. The excitations in the staggered configuration, with $Q = \pi$, are given by

$$\omega_{s(1,2)}(k) = \frac{\sqrt{\Delta^2 + 2J^2 \pm 4\Delta J\sin(k) - \cos(2k)\,(t^2 - \Delta^2) + t^2}}{\sqrt{2}}, \quad (3.11)$$

and $\omega_{s(3,4)}(k) = \pm\omega_{s(2,1)}(k)$. Notice that the condition $\mu = E_F = 0$ implies that for the non-interacting system, the band of conduction electrons is half-filled. The number of localized f-electrons is arbitrary, $n_f \leq 1$, and does not affect the total energy of the system, when $J = 0$. In Fig. 3.1 we plot the dispersion relations of the full problem, Eqs. 3.10 and 3.11, for specific values of parameters Δ and J, of the homogeneous and staggered configurations. For completeness, we also show the dispersions of the pure Kitaev chain ($J = 0$). In the homogeneous case of Fig. 3.1a, the gap closes for $J/t = 1$, independent of Δ. In the staggered case, Fig. 3.1b, the gap in the dispersions closes for $J = \Delta$. In Section IV, to fully describe the topological properties of the interacting system, we investigate numerically the case of finite chains with open boundary conditions. We obtain the spectrum of eigenvalues and the wave functions of the MZMs. However, before that we discuss briefly the pure one-dimensional spinless FK model, since its properties will be relevant for understanding the superconducting case. Notice that this model corresponds to taking the superconducting gap $\Delta = 0$ in Eq. 3.1.

4 The one-dimensional spinless Falicov-Kimball model ($\Delta = 0$)

The FK model is a well studied strongly correlated electronic problem, with many applications ranging from heavy fermions to metal-insulator and valence transitions [21]. In particular the one-dimensional spinless FK model has many well-known properties. It can be approached using the technique of bosonisation that yields exact results. From the point of view of topological properties this model is completely trivial. In this section we briefly discuss the spinless one-dimensional FK model and emphasize some aspects that are relevant when considering the full superconducting problem. Formally, we just take the amplitude of the superconducting pairing $\Delta = 0$, to obtain the dispersion relations for the homogeneous and staggered phases of the model. It is possible to distinguish two situations depending on the value of the ratio (J/t).

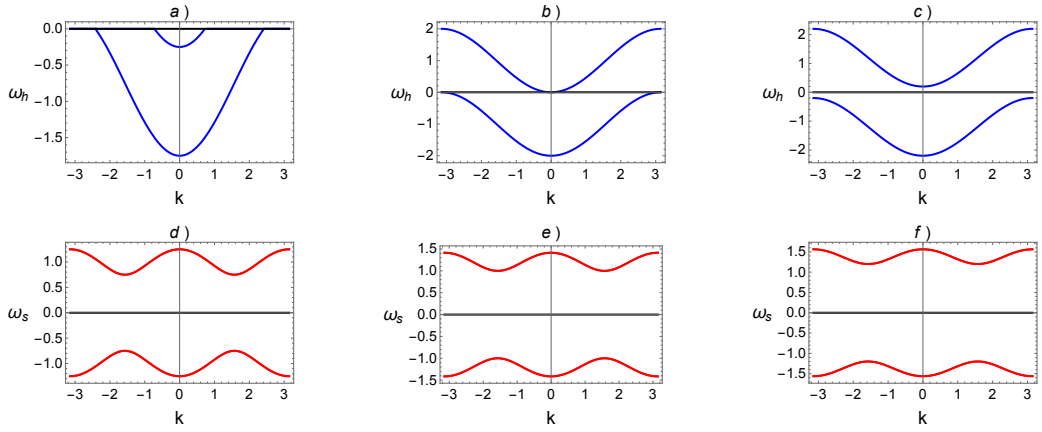

Figure 3.2: Dispersion relations of the FK model ($\Delta = 0$). Homogeneous case, $\omega_h(k)$ for a) $J/t = 0.75$, b) $J/t = 1$ and c) $J/t = 1.2$. Staggered configuration, $\omega_s(k)$ for d) $J/t = 0.75$, e) $J/t = 1$ and f) $J/t = 1.2$. In the homogeneous case, a) corresponds to a metallic state and at b) $J/t = 1$ there is a metal insulator transition. In the staggered configuration the system is always insulating. The black line is the energy of the localized quasiparticles that coincides with the chemical potential.

For $J/t > 1$, both homogeneous and staggered configurations correspond to insulating phases, as shown in Figs. 3.2c and 3.2f. Conversely, for $J/t < 1$, the homogeneous configuration corresponds to a metallic phase, Fig. 3.2a, but the staggered one remains insulating, as can be seen in Fig. 3.2d. Then for the homogeneous case, with one localized electron per site ($n_f = 1$), there is a metal-insulator transition at $|J/t| = 1$, as shown in Fig. 3.2b for the dispersion relations. The staggered phase is always insulating. Notice that the presence of two dispersive bands is due to an effective hybridization between the localized level and the conduction band due to the FK interaction. If this is too large it can open a gap and give rise to a metal-insulator transition Due to the condition $E_f = \mu = 0$, the energy of the pure f-electron system does not depend on the number of f-electrons, differently from the coupled $s - f$ system. In Fig. 3.3 we show the ground state energies of the special configurations, $Q = 0$ and $Q = \pi$, as functions of the interaction J. Notice that the staggered configuration has a lower energy compared

to the homogeneous one. When $\langle n_f \rangle = 1/2$, besides ordered configurations, as the staggered and other types of superlattices [124], there are many disordered configurations [21, 49], corresponding to a random arrangement of the local moments in the chain. In Fig. 3.3 we also show the ground state energies, as functions of the interaction J, for several realizations of random configurations with $\langle n_f \rangle = 1/2$. The disordered configurations have a probability $p = 1/2$ for a site being occupied, by a localized f-electron. The ordered, staggered configuration is always the one with lower energy.

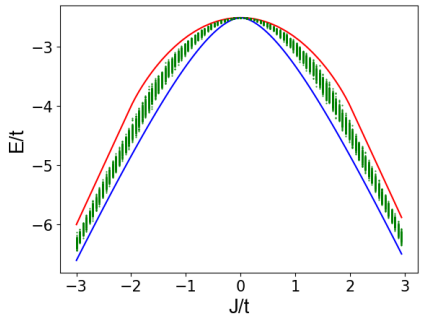

Figure 3.3: (Color online) Ground state energy of the spinless FK model ($\Delta = 0$). Homogeneous case, $n_f = 1$ (red), staggered, $n_f = 1/2$ (blue) and random configurations (green) with $\langle n_f \rangle = 1/2$. Notice that, the staggered configuration has an energy lower than all the probed random configurations with $\langle n_f \rangle = 1/2$.

5 Analysis of the dispersion relations and density of states

We now return to the full problem consisting of a band of spinless fermions, with p-wave pairing, that interacts with a background of localized f-electrons, Eq. 3.1. The Hamiltonian with $J = 0$, corresponds to a Kitaev chain and an independent collection of localized electrons. On the other hand, for $\Delta = 0$, we obtain the FK model. The topological properties of the Kitaev chain are well known, it presents a non-trivial topological phase, for $|\mu/2t| < 1$, with Majorana modes at its ends [3]. In the present case the chemical potential $\mu = 0$, such that the Kitaev chain is in a topological superconducting phase [3]. We now turn on the interaction with the localized f-electrons and study its effects.

We start discussing the results of Fig. 3.1 for the dispersion relations, Eqs. 3.10 and 3.11, and the density of states obtained from these dispersions shown in Fig. 3.5. We consider both, the homogeneous and staggered configurations and take $\Delta/t = 0.2$ in the figures. In the homogeneous case, the gap closes at $J/t = 1$, as can be seen in the density of states shown in Fig. 3.5a. For $J \neq 1$ the superconductor is gapped, as can be obtained directly from the dispersion relations and as shown in the density of states in Fig. 3.5a. However, there is a fundamental difference between the cases $J/t < 1$ and $J/t > 1$, as we discuss below using numerical results in finite chains.

To better understand, a property that we can calculate is the WN, which is the topological invariant that is discussed in the appendix C. In figure 3.4, we take $\Delta = 0.2$ for different values of J and

t for the homogeneous chain. Note that when J>t the winding number is zero, when J=t the system is in the phase transition, and when J<t the chain has two edge states, which is in line with the result obtained in the density of states.

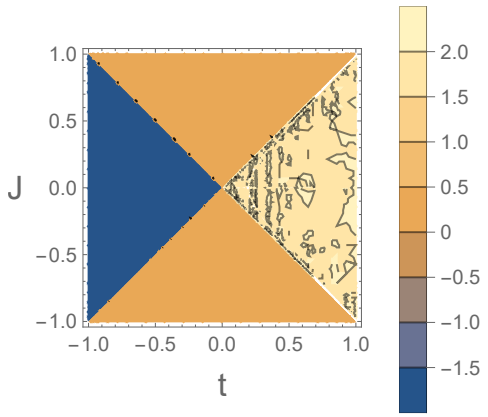

Figure 3.4: $\Delta = 0.2$,Q=0, in the blue region WN=-2, in yellow WN=2 and in mustard WN=0

Fig. 3.5b shows the density of states at the gap closing point of the homogeneous case for different values of the coupling Δ. As the pairing interaction is turned on, a competition between the localization due to FK interactions and the formation of p-wave pairs occurs; the peak decreases as the superconducting pairs are formed, as indicated in the inset of the figure, and the density of states approaches that of a renormalized uncorrelated tight-binding chain. For comparison, we also show in Fig. 3.5b the tight-binding density of states for $J/t = \Delta/t = 0.0001t$.

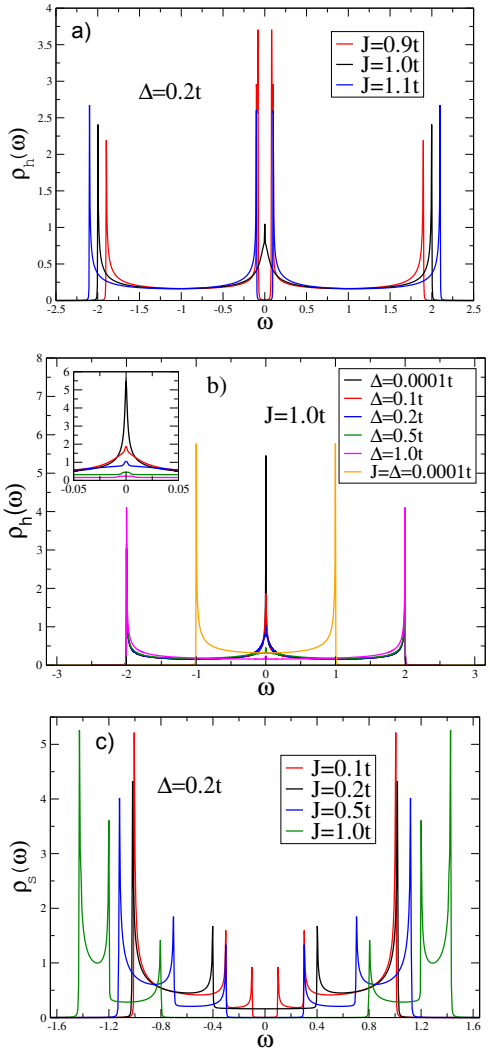

Figure 3.5: Density of states in the superconducting state. a) for the homogeneous case with $\Delta/t = 0.2$ and different values of the coupling parameter J/t, below, at, and above the gap closing transition. b) for the homogeneous case at the gap closing transition and different pairing amplitudes Δ/t. The inset shows the density of states close to $\omega = 0$. c) for the staggered configuration as a function of J/t and fixed $\Delta/t = 0.2$.

In the staggered configuration, the gap closing occurs at $J = \Delta$ and the superconductor is gapped, whenever $J \neq \Delta$, as shown in Fig. 3.5c for the density of states. Notice that there is a finite density of states at $\mu = 0$ for $J = \Delta$, where the system is gapless. This is similar to the corresponding density of states of an armchair nano-ribbon, whenever $N = 3M - 1$, with M being integer [126]. Like in the homogeneous case, in the staggered phase the gapped phases, for $J > \Delta$ and $J < \Delta$ are distinct with respect to their topological properties, as we discuss next.

6 Topological properties of finite chains

In order to investigate the topological properties of the interacting system, instead of calculating a topological invariant [50, 52, 124] and using the bulk-boundary correspondence principle [126], we opt to study numerically the behavior of interacting finite chains with open boundary conditions. In this approach the appearance of zero energy edge states gives direct evidence of the non-trivial topological character of the system.

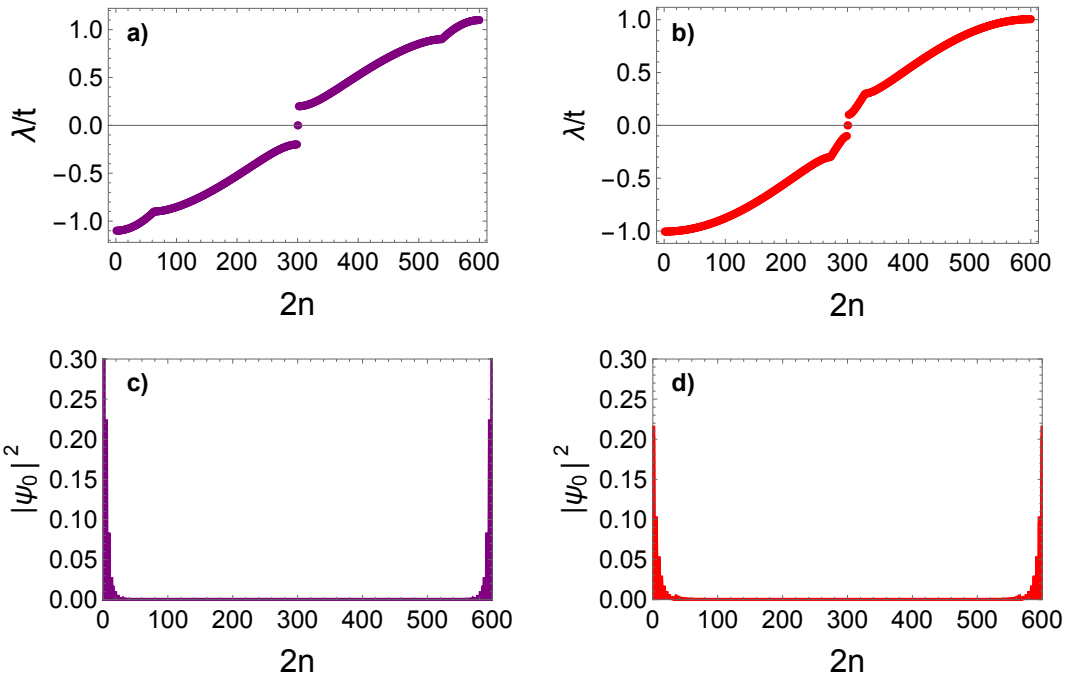

Figure 3.6: (Color online) Eigenvalues λ/t for a chain of 300 sites for $t = 1$, $\Delta/t = 0.2$, a) in the homogeneous phase, for $J/t = 0.1 < 1$, b) in the staggered phase for $J/t = 0.1 < \Delta/t$. In c) and d) we show the amplitude square of the wave functions of the corresponding zero modes for the homogeneous and staggered phases, respectively.

In Fig. 3.6 we show the eigenvalues for a chain of 300 sites for both homogeneous and staggered configurations. In the homogeneous chain, Fig. 3.6a, superconductivity is gapped, with zero energy modes that persist, as long as $J < t$. These zero modes are edge states as can be seen directly from their wave functions shown in Fig. 3.6c. At $J/t = 1$ the gap closes and the system is a gapless superconductor [125]. For $J > t$, the gap reopens as shown in Fig. 3.8a, but the zero energy edge states disappear, indicating that the superconductor is topologically trivial . Recall that in the absence of pairing, the homogeneous FK chain is metallic for $J/t < 1$, as shown in Fig. 3.2a, such that topological superconductivity arises from a metallic state. Then in the homogeneous case there is a topological phase transition together with a gap closing, at $J/t = 1$.

In the staggered case, the topological superconducting phase, characterized by the presence of zero energy edge states, exists for $J < \Delta$, as shown in Fig. 3.6b and Fig. 3.6d. At $J = \Delta$ the superconductor is gapless and above this critical value, the superconducting chain is gapped and topologically trivial with no zero modes, as shown in Fig. 3.8b. In the staggered case, as we turn on the superconducting pairing, non-trivial topological superconductivity emerges from an insulating phase (see Fig. 3.2d) of the FK model, as soon as, the pairing amplitude becomes larger than J.

Analogously to what was done for the homogeneous chain case,in the figure 3.7 we also calculate the WN of the staggered chain ($Q = \pi$), take $\Delta = 0.2$ and vary J and t. Note that when $J < \Delta = 0.2$ the system always has edge states. The phase transition occurs at $J = \Delta$ and when $J > \Delta$ the system has no edge states, which is again in agreement with what is obtained in the density of states.

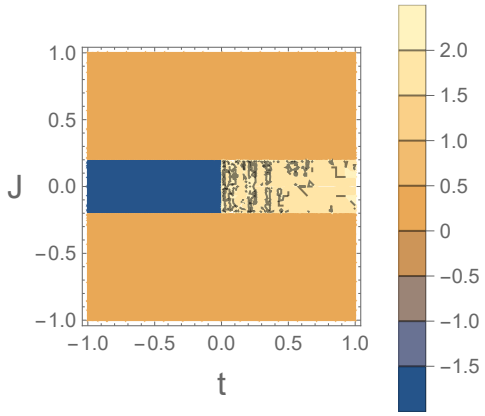

Figure 3.7: $\Delta = 0.2$,$Q = \pi$, in the blue region WN=-2, in yellow WN=2 and in mustard WN=0

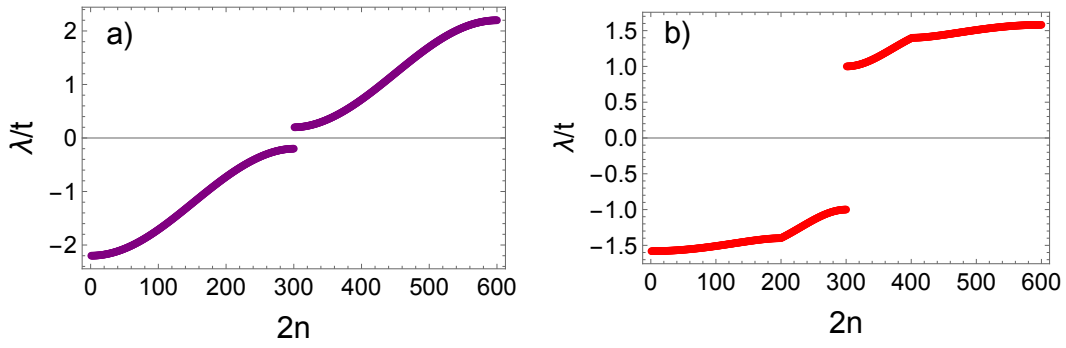

Figure 3.8: (Color online) Eigenvalues λ/t for a chain of 300 sites for $t = 1$ and fixed $\Delta/t = 0.2$, a) in the homogeneous phase, for $J/t = 1.3 > 1$, b) in the staggered phase for $J/t = 1.2 > \Delta/t$. Both phases are gapped and topologically trivial superconductors as indicated by the absence of zero energy edge modes.

Then, the topological phase transition occurs for $J/t = 1$ in the homogeneous case and for $J/\Delta = 1$ in the staggered case.

7 Random occupation of the local moments in the chain

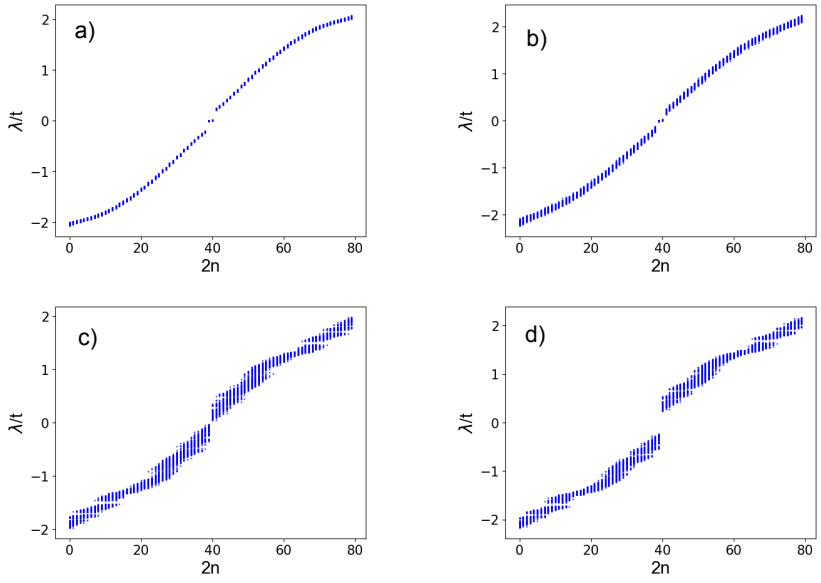

Figure 3.9: Eigenvalues λ/t for $\Delta/t = 0.2$, corresponding to 200 realizations of random configurations for a chain with 40 sites, with probability $p = 1/2$ for a site being occupied by a localized electron ($\langle n_f \rangle = 1/2$). a) for $J/t = 0.1$, b) for $J/t = 0.3$, c) for $J/t = 1$ and d) for $J/t = 1.2$ The zero modes persist all the way to the topological phase transition of the homogeneous case at $J/t = 1$.

The problem of topological phases in random chains is complex and requires a closer examination. The existence of zero modes in chains with $p = 1/2$ for $(J/t) \leq 1$ does not necessarily imply the topological

character of the chain in this region of the phase diagram. We find that in some configurations, with zero modes their wave-functions are not localized at the edges of the chain, but in the bulk. In order to establish the topological character of the random chains a more detailed analysis is necessary. For this purpose we consider a transfer matrix approach [50–52] that has been used in the study of localization in random chains with different types of disorder [51]. This allows to define a Lyapunov exponent that can distinguish between trivial and topological phases of the superconducting chain.

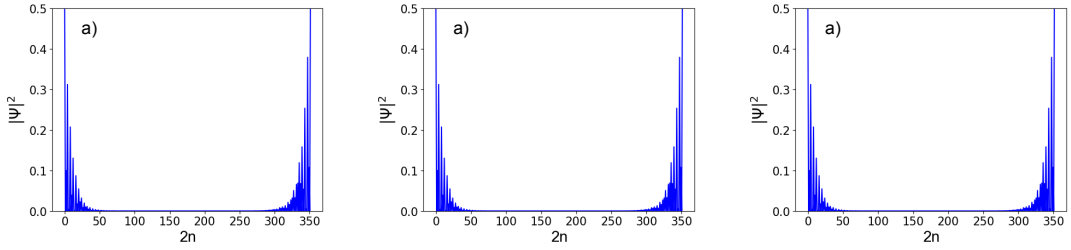

Figure 3.10: Amplitude square of the wave functions of the lower energy modes of a chain with 180 sites for fixed $\Delta/t = 0.2$, with probability $p = 1/2$ for a site being occupied by a localized electron ($\langle n_f \rangle = 1/2$) and particular realizations of disorder. a) $J/t = 0.1$. b) $J/t = 0.3$. c) Amplitude of the wave-function of the ordered staggered configuration with $J/t = 0.1$. Compare with a) and notice that in the random case the wave function is more localized.

The Heisenberg equation of motion for the Majorana operators α_A in the Hamiltonian, Eq. 3.1 can be cast in the form of a recursion relation [50, 52, 124],

$$\begin{pmatrix} \alpha_{An+1} \\ \alpha_{An} \end{pmatrix} = T_i \begin{pmatrix} \alpha_{An} \\ \alpha_{An-1} \end{pmatrix},$$

with a similar equation for the α_B. The relevant, zero energy, site dependent transfer matrix is given by,

$$T_i(E=0) = \begin{pmatrix} \frac{-2J_i/t}{1+\Delta/t} & \frac{-(1-\Delta/t)}{1+\Delta/t} \\ 1 & 0 \end{pmatrix}.$$

Notice that we can write the interaction between localized and conduction electrons at a given site i of the chain, as $J_i = Jx_i$ where $x_i = \pm 1$ according to the probability distribution, $P(x_i) = p\delta(x_i - 1) + (1 - p)\delta(x_i + 1)$ for a given site. The ratio $r_i = (\alpha_{Ai+1}/\alpha_{Ai})$, as can be seen from the transfer matrix, obeys the following recursion relation [51],

$$r_{i+1} = -\frac{2(J/t)x_i}{1 + (\Delta/t)} - \frac{1 - (\Delta/t)}{1 + (\Delta/t)} \frac{1}{r_i}. \tag{3.12}$$

This is a random map since the x_i take random values in different sites. We remark, the following relation involving the r_i,

$$\prod_{i=1}^{N} r_i = \frac{\alpha_{N+1}}{\alpha_N} \frac{\alpha_N}{\alpha_{N-1}} \frac{\alpha_{N-1}}{\alpha_{N-2}} \cdots \frac{\alpha_1}{\alpha_0} = \frac{\alpha_{N+1}}{\alpha_0}, \tag{3.13}$$

where we dropped the symbol A from the operators α. The quantity above describes the behavior of the amplitude of the wave functions of the edge modes as it penetrates in the chain. It can be used to define

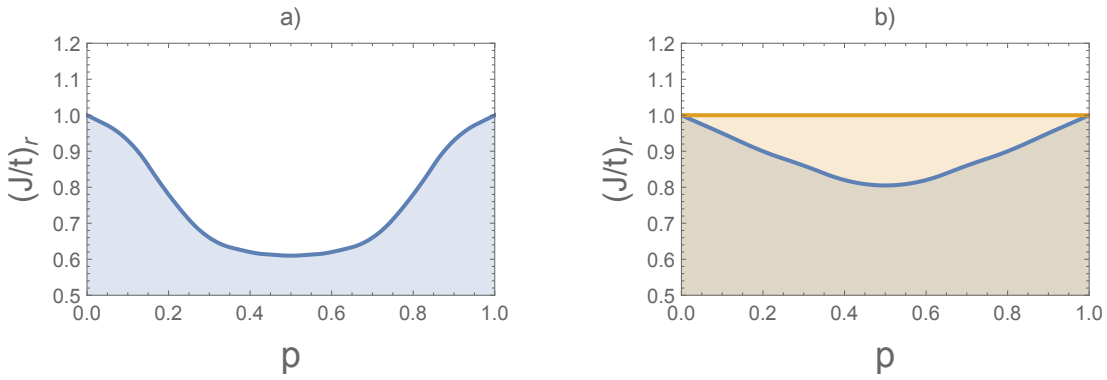

Figure 3.11: Phase diagram of chains with probability p of its sites being occupied by a local moment. The lines in the figures represent the boundaries between trivial and topological phases and correspond to the points where the Lyapunov exponent γ_r, changes sign. The filled regions are topologically non-trivial, with $\gamma_r < 0$. a) for $\Delta/t = 0.2$. b) $\Delta/t = 0.5$. In b) the horizontal orange line is the phase boundary for $\Delta/t = 1$.

a Lyapunov exponent,

$$\gamma_r = \frac{1}{N}\sum_{i=1}^{N} \ln |r_i|. \tag{3.14}$$

We have calculated numerically this Lyapunov exponent using Eq. 3.12 to determine the phase diagrams of random chains with different values of Δ/t, J/t and p. The topological region of the phase diagram is characterized by negative values of the Lyapunov exponents and the phase boundary is where these change sign. We carried out 15×10^4 iterations of Eq. 3.12 with $r_0 = 1$ to obtain the phase diagrams shown in Figs. 3.11 and 3.12. Notice that for $\Delta/t = 1$, the Lyapunov exponent can be calculated exactly. Since the product of the x_i can only assume the values, $\prod x_i = \pm 1$, we have $\gamma_r = \ln[|J/t|]$ independently of the probability p. This implies that the system is topological, whenever $J/t < 1$, for any p. We point out that between the phase boundaries for $\Delta/t = 1$ (yellow line) and $\Delta/t = 1/2$ (blue line) in Fig. 3.11b, we still observe zero modes in the spectra of eigenvalues, but the system is not topological in this region. For some of these modes we find that their wave functions are localized in the bulk of the chain. Finally, Fig. 3.12 gives the phase diagram for a fixed value of $p = 1/2$ showing the phase boundary for the disordered chain. In this figure the straight line is the critical line for the ordered staggered configuration. Notice that disorder increases the range of the topological phase in the phase diagram. Finally, we should mention that if we use an alternative approach, and define a Lyapunov exponent from the product of the transfer matrices [124], we obtain similar results.

we studied the properties of the one-dimensional FK model with a p-wave pairing of the electrons in the conduction band. We have shown that this many-body problem can be mapped in a non-interacting one, which allows it to be exactly soluble. The solution provides a clear picture of the effects of interactions and disorder in the topological properties of the superconducting chain. The conditions for solubility are quite general, and permits to treat different numbers of localized electrons in the chain and arbitrary values

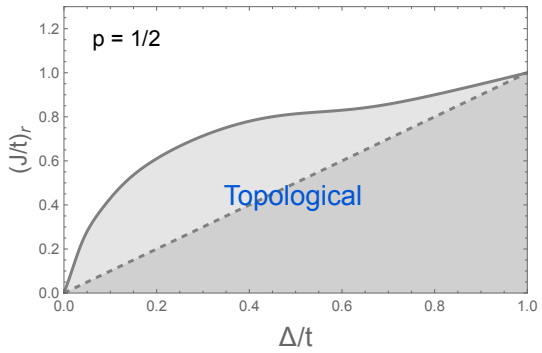

Figure 3.12: Phase diagram showing the critical coupling as a function of the gap amplitude for a fixed probability, $p = 1/2$, of occupation of a site by a local moment. The straight, dashed line is the phase boundary of the ordered staggered configuration. Disorder extends the topological region of the phase diagram.

of the FK interaction and superconducting pairing. In this paper we focused in a half-filled conduction band but the solution can be easily extended for general occupations. We find that for a chain with a homogeneous configuration of localized electrons, i.e., with every site of the chain occupied by a local moment, the FK interaction leads eventually to a suppression of the superconducting topological phase, at large values of J ($J_c = t$). In this system when turning on the pairing interaction, superconductivity arises from a metallic state of the FK model. When the localized electrons assume a staggered configuration, in which every other site in the chain is occupied, the critical value of the coupling to suppress the topological phase is much reduced, being given by the pairing energy of the conduction electrons ($J_c = \Delta$). In this case, superconductivity arises from an insulating state of the FK model, and we can alternatively state that a minimum critical value of the pairing amplitude, $\Delta_c = J$, is required to induce superconductivity in the insulator. The staggered configuration corresponds to $\langle n_f \rangle = 1/2$. For this occupation of local moments, most of the configurations are disordered, with the localized electrons randomly occupying the sites in the chain. We have used transfer matrices and exact recursion relations to obtain the Lyapunov exponents and show that for $p = 1/2$, randomness extends the range of stability of the topological superconducting phase with respect to the coupling to the localized electrons. While in the ordered staggered configuration, the topological superconducting phase exists for $J/\Delta < 1$, in the presence of disorder, it is stable up to larger values of J, as shown in Fig. 3.12. We have also studied random configurations with an arbitrary probability p for a site in the chain being occupied by a localized electron. The results obtained from the Lyapunov exponents yield the phase diagrams of the model and allows to put on firm grounds the role of interaction and disorder in the topological properties of an archetypal system, namely the Kitaev chain. Finally, an interesting challenge is to include in this problem the hybridization between the localized and itinerant electrons, which gives rise to the quantum Falicov-Kimball model [21]. We could also investigate the thermoelectric properties of these systems at the topological quantum phase transition of the homogeneous ($t = \Delta$) and staggered ($J = \Delta$), cases [127].

Chapter 4

Conclusions and perspectives

In Chapter 2, we examine monoatomic and diatomic sp-chains that directly map onto the SSH and RM models, respectively. We derive the density of states at the edge of a semi-infinite chain, which depends on the chain's topological phase. Our results indicate that the weight of zero-energy modes in the non-trivial topological phase continuously diminishes as the system moves away from the topological transition.

To investigate transport properties, we model a device comprising a quantum dot coupled to two identical semi-infinite SP or RM chains. At zero temperature and away from the topological transition, the current through the device is zero because the chains behave as bulk insulators, regardless of their topological phase. However, at finite temperatures, activated transport emerges, differing between trivial and topological phases. This study focuses on the linear response regime (zero voltage limit). Extending this analysis to finite voltages would require the Keldysh formalism [120], a direction we leave for future research.

At the topological transition of monoatomic (SSH) chains and zero temperature, the conductance reaches a universal value $G/G_0 = 1$, independent of model parameters such as chain-dot coupling, provided the dot energy $E_0 = 0$. Since edge states delocalize into the bulk at the transition, the system conducts even at $T = 0$. The normalized WF ratio equals unity (in terms of the Lorenz number), while the thermal conductivity vanishes at $T = 0$. Due to particle-hole symmetry, the thermopower of monoatomic chains remains zero.

Diatomic sp-chains with sublattice energy differences exhibit different behavior. Here, the broken chiral symmetry (absent in the SSH model) leads to a RM Hamiltonian, yet non-trivial topological phases characterized by Chern numbers persist. Notably, at the topological transition, the zero-temperature conductance is $G/G_0 = 1/2$, suggesting fractional charge carriers a consequence of chiral symmetry breaking.

The thermopower also deviates from the SSH case: it remains non-zero at low temperatures, reaching a universal value at $T = 0$ consistent with fractional charges $q^* = 1/2$. This arises from zero-energy mode degeneracy. Comparisons with Majorana modes in p-wave superconductors [121] could yield

further insights.

Unlike spin-orbit coupling, the antisymmetric hybridization in these chains does not mix carrier spins, facilitating spin-polarized materials. Moreover, sp-chains with edge modes are experimentally more accessible than p-wave superconductors. Carbyne, a 1D carbon allotrope with sp hybridization, realizes such chains. Their tunable properties, including high thermoelectric efficiency at elevated temperatures (via V_1/V_2 adjustment), make them promising for applications.

In Chapter 3, we analyze the 1D FK model with p-wave pairing in the conduction band. This many-body problem maps to a non-interacting system, permitting an exact solution that clarifies how interactions and disorder affect the superconducting chain's topology. While we focus on a half-filled band, our solution generalizes to arbitrary fillings. For homogeneous localized-electron configurations (all sites occupied), the FK interaction suppresses the topological superconducting phase at large $J(J_c = t)$. Here, pairing induces superconductivity from a metallic FK state. In contrast, for staggered configurations (alternating occupied sites, $<nf> = 1/2$, the critical coupling drops to $J_c = \Delta$, with superconductivity emerging from an insulating FK state. Equivalently, a minimum pairing $\Delta_c = J$ is needed to induce superconductivity.

One possible direction for exploring the exact solution of the FK model is to consider the more general case where $\mu = E_f \neq 0$. We have obtained an analytical solution for this case, but we have not yet studied the problem numerically.

Disordered configurations (random site occupations at p=1/2) were studied via transfer matrices and Lyapunov exponents. Disorder enhances the topological phase's stability: while the ordered staggered case requires $J/\Delta < 1$, disorder permits larger J (Fig. 3.12). Phase diagrams for arbitrary p confirm the interplay of interactions and disorder in the Kitaev chain's topology. Future work could incorporate localized-itinerant electron hybridization (quantum FK model [21]) or explore thermoelectric properties at topological transitions (homogeneous $t = \Delta$; staggered $J = \Delta$) [127].

Another route to explore with the systems studied in this Thesis is their non-Hermitean counterparts. There is an effort in the literature to investigate these types of systems [128,129]. Even though the SSH and RM models, when seen from this new perspective, reveal novel characteristics such as the non-Hermitean skin effect. This phenomenon occurs when a substantial number of eigenstates—indeed, all eigenstates in a one-dimensional chain with non-reciprocal coupling—of a non-Hermitian system under open boundary conditions (OBC) become exponentially localized at one boundary (edge) of the system.

In Hermitean systems, the validity of the BBC is guaranteed: This means that topological invariants calculated for a system with PBC - effectively a loop directly predict the number of robust edge states under open boundary conditions (OBC - a finite chain). On the contrary, in non- Hermetian systems [130], the topological invariant derived from the PBC Hamiltonian (the winding number of the complex loop) no longer accurately predicts the number of edge states under OBC. To address this, a new framework, known as the non-Bloch band theory or generalized Brillouin zone (GBZ) theory, is required to restore the modified Bloch band theory.

The skin effect necessitates a complete reevaluation of how we classify topological phases in non-

Hermitian systems. Topology must now be defined based on the OBC spectrum or the GBZ, leading to new invariants and phase diagrams.

Appendix A

Effective potential method for surfaces

Consider a semi-infinite monoatomic chain with interaction V between the first neighbors described by the following Hamiltonian:

$$\mathcal{H} = -\sum_i V|i\rangle\langle i+1| + V|i+1\rangle\langle i|,$$

which is represented in matrix form as:

$$\mathcal{H} = -\begin{Bmatrix} 0 & V & 0 & 0 & . \\ V & 0 & V & 0 & . \\ 0 & V & 0 & V & . \\ 0 & 0 & V & 0 & . \end{Bmatrix}.$$

With the Hamiltonian defined it is possible to calculate the Green's function through the equation

$$G = (E - \mathcal{H})^{-1}, \tag{A.1}$$

we thus obtain the matrix associated with Green's function which is given by:

$$G = \begin{Bmatrix} E & V & 0 & 0 & . \\ V & E & V & 0 & . \\ 0 & V & E & V & . \\ 0 & 0 & V & E & . \end{Bmatrix}. \tag{A.2}$$

Using the definition given by the equation A.1, and indexing from 0 to ∞ with 0 being the surface atom, the Green's function on the surface is defined by :

$$g = \langle 0|G|0\rangle_s = \frac{1}{(E-h)}, \tag{A.3}$$

where $h(E)$ is an eigenenergy representing one side of the chain. Therefore the Green's function of the "bulk" of an atom inserted in an infinite chain is described by:

$$g' = \langle 0|G|0\rangle_b = \frac{1}{(E-2h)}, \tag{A.4}$$

the factor 2 arises because there are two self-energies, one associated with the left side of the chain and the other with the right side of it. Using the equations A.3 and A.4 we have a relationship between g and g':

$$E + \frac{1}{g'} = \frac{2}{g}.$$

The effective potential h can be calculated using the equations A.2 and A.3 using the Foo-Thorpe's method [89]:

$$g = \frac{1}{(E-h)} = \begin{Bmatrix} E & V \\ V & E-h \end{Bmatrix}^{-1}_{00},$$

but $(E-h) = g^{-1}$ therefore:

$$g = \begin{Bmatrix} E & V \\ V & g^{-1} \end{Bmatrix}^{-1}_{00}, \tag{A.5}$$

Calculating the inverse we have:

$$g = \frac{1}{(E/g - V^2)} \begin{Bmatrix} g^{-1} & -V \\ -V & E \end{Bmatrix}_{00}.$$

Let us take the terms of the matrix associated with the zero site:

$$(Vg)^2 - 2\alpha V g + 1 = 0,$$

where $\alpha = \frac{E}{2V}$, we now just need to calculate the roots of the second-degree equation to obtain Green's function:

$$g = \frac{1}{V}(\alpha \pm \sqrt{\alpha^2 - 1}).$$

The Green's function for all other atoms can be easily obtained using the notation defined in the equation A.5, we can extend the method to any level such that :

$$g = \begin{Bmatrix} E & V & 0 \\ V & E & V \\ 0 & V & g^{-1} \end{Bmatrix} = \begin{Bmatrix} E & V & 0 & 0 \\ V & E & V & 0 \\ 0 & V & E & V \\ 0 & 0 & V & g^{-1} \end{Bmatrix}.$$

Appendix B

Winding Number calculation

In this appendix will introduce the WN [131] which corresponds to the number of edge states in the topological insulator chain. Through this topological invariant we can verify in which topological phase the system is. Here we will explain in detail how to calculate the WN:

1 - Express the Hamiltonian of the system in terms of k's:

Let us consider the Hamiltonian of the SSH chain defined by the equation 2.11

$$\begin{aligned} H_{SSH}(n) = -V_1 \sum_{\infty}^{\infty} (|n,2\rangle \langle n,1| + |n,1\rangle \langle n,2|) \\ -V_2 \sum_{\infty}^{\infty} (|n+1,1\rangle \langle n,2| + |n,2\rangle \langle n+1,1|) \end{aligned} \tag{B.1}$$

Using the fourier transform on the equation B.1 we have

$$\begin{aligned} H_{SSH}(k) = -V_1 \sum_{\infty}^{\infty} (|k,2\rangle \langle k,1| + |k,1\rangle \langle k,2|) \\ -V_2 \sum_{\infty}^{\infty} (e^{-ik} |k,1\rangle \langle k,2| + e^{ik} |k,2\rangle \langle k,1|) \end{aligned} \tag{B.2}$$

in matrix notation the equation B.2 is given by

$$H_{SSH}(k) = \begin{pmatrix} 0 & -V_1 - V_2 e^{ik} \\ -V_1 - V_2 e^{-ik} & 0 \end{pmatrix}$$

$$H_{SSH}(k) = \begin{pmatrix} 0 & h(k) \\ h^*(k) & 0 \end{pmatrix}$$

where $h(k) = -V_1 - V_2 e^{ik}$.

2 - Find the matrix K that anti-commutes with H(k) ($H(k)K + KH(k) = 0$):

It is

$$K = \begin{pmatrix} a & b \\ c & d \end{pmatrix}$$

$$[H(k), K] = \begin{pmatrix} 0 & h(k) \\ h^*(k) & 0 \end{pmatrix} \begin{pmatrix} a & b \\ c & d \end{pmatrix} + \begin{pmatrix} a & b \\ c & d \end{pmatrix} \begin{pmatrix} 0 & h(k) \\ h^*(k) & 0 \end{pmatrix} = \begin{pmatrix} 0 & 0 \\ 0 & 0 \end{pmatrix}$$

also using that the matrix K has to be unitary we conclude that

$$K = \begin{pmatrix} 1 & 0 \\ 0 & -1 \end{pmatrix}$$

3 - Calculate the eigenvectors of the matrix k:

In this example the eigenvectors are calculated

$$\rho_1 = \begin{pmatrix} 1 \\ 0 \end{pmatrix}, \rho_2 = \begin{pmatrix} 0 \\ -1 \end{pmatrix} \tag{B.3}$$

4 - Define the matrix U with the eigenvectors of K:

Using B.3 we then define the matrix U

$$U = \begin{pmatrix} 1 & 0 \\ 0 & -1 \end{pmatrix}$$

5 - Calculate the Hamiltonian $H(A(k))$:

Using the matrix U we obtain the matrix H(A(k)) using $U^\dagger H(k)U = H(A(k))$

$$U^\dagger H(k)U = \begin{pmatrix} 1 & 0 \\ 0 & -1 \end{pmatrix} \begin{pmatrix} 0 & h(k) \\ h^*(k) & 0 \end{pmatrix} \begin{pmatrix} 1 & 0 \\ 0 & -1 \end{pmatrix}$$

$$U^\dagger H(k)U = \begin{pmatrix} 0 & -h(k) \\ -h^*(k) & 0 \end{pmatrix}$$

where

$$H(A(k)) = \begin{pmatrix} 0 & A(k) \\ A^*(k) & 0 \end{pmatrix}$$

with $A(k) = -h(k)$.

6 - Calculate the winding number:

With A(k) defined we can now calculate the WN using the formula

$$w = -1/2i\pi \int_{-\pi}^{\pi} dk \partial k ln(DetA(k))$$

$$w = 1/2\pi \int_{-\pi}^{\pi} dk \frac{eik}{e^{ik} - \mathcal{S}}$$

where $\mathcal{S} = -\frac{V_1}{V_2}$.

Appendix C

Calculation of thermoelectric coefficients

In this chapter we will calculate the coefficient L_0 in detail to understand how the other calculations were made.

We will start by defining the Fermi-Dirac distribution

$$n_f(w) = \frac{1}{e^{\frac{w}{T}} + 1},$$

Let us now consider the Green's function of the SSH chain

$$G_0(E) = \frac{1}{2V_2^2 E}((E^2 + V_2^2 - V_1^2) \pm (((E^2 + V_2^2 - V_1^2)^2 - 4E^2V_2^2)^{\frac{1}{2}})),$$

considering $w = \frac{E}{V_2}$ and $V = \frac{V_1}{V_2}$ we have

$$G_0(w) = \frac{1}{2w}((w^2 + 1 - V^2) \pm (((w^2 + 1 - V^2)^2 - 4w^2)^{\frac{1}{2}})),$$

considering $d = 1 - V^2$ we have

$$G_0(w) = \frac{1}{2w}((w^2 + d) \pm (((w^2 + d)^2 - 4w^2)^{\frac{1}{2}})),$$

taking $w = w' + i\varepsilon$

$$G_0(w) = \frac{1}{2}((w' + \frac{dw'}{w'^2 + \varepsilon^2} + i(\varepsilon - \frac{d\varepsilon}{w'^2 + \varepsilon^2}) \pm \frac{(((w^2 + d)^2 - 4w^2)^{\frac{1}{2}})}{w}),$$

but $\delta(w) = \frac{1}{\pi}\frac{\varepsilon}{w^2 + \varepsilon^2}$

$$G_0(w) = \frac{1}{2}((w' + \frac{dw'}{w'^2 + \varepsilon^2} + i(\varepsilon - d\pi\delta(w)) \pm \frac{(((w^2 + d)^2 - 4w^2)^{\frac{1}{2}})}{w}),$$

taking the imaginary $G_0(w)$ e $\varepsilon \to 0$

$$ImG_0(w) = \frac{1}{2}(-d\pi\delta(w) + Im(ReG_d(w) + iImG_d(w))Im(\frac{1}{w' + i\varepsilon}),$$

where $G_d(w) = ((w^2 + d)^2 - 4w^2)^{\frac{1}{2}}$

$$ImG_0(w) = \frac{1}{2}(-d\pi\delta(w) + Im(ReG_d(w) + iImG_d(w))Im(\frac{w'}{w'^2+\varepsilon^2} - i\pi\delta(w)),$$

taking one more time $\varepsilon \to 0$:

$$G_i = ImG_0(0) = \frac{-\pi}{2}(d\delta(0) + ReG_d(0)\delta(0) + \frac{ImG_d(0)}{w}),$$

but $ReG_d(0) = (((0)^2+d)^2 - 4(0)^2)^{\frac{1}{2}} = |d|$ then

$$G_i = ImG_0(0) = \frac{-\pi}{2}(d + |d|).$$

Let us now calculate the real part of Green's function

$$ReG_0(w) = \frac{1}{2}(Re(w + \frac{d}{w}) \pm Re(ReG_d(w) + iImG_d(w))Re(\frac{1}{w})),$$

taking $w = w' + i\varepsilon$

$$ReG_0(w) = \frac{1}{2}(w' + \frac{dw'}{w'^2+\varepsilon^2}) \pm Re(\frac{w'ReG_d(w)}{w'^2+\varepsilon^2} + \frac{w'iImG_d(w)}{w'^2+\varepsilon^2} + iReG_d(w)\pi\delta(w) + ImG_d(w)\pi\delta(w)),$$

taking $\varepsilon \to 0$

$$G_r = ReG_0(0) = \frac{1}{2}(w' + \frac{d}{w'}) + \frac{|d|}{w'},$$

Using

$$G_\lambda^\sigma = \begin{pmatrix} (G_\lambda^{0\sigma})^{-1} & V \\ V & (G_s^\sigma)^{-1} \end{pmatrix}^{-1}$$

where

$$G_\lambda^{0\sigma} = (w - \varepsilon_\sigma)^{-1}$$

and the Greenian of the electrons in the isolated chain is given by:

$$G(0) = \frac{1}{w - \varepsilon - V^2 G_0},$$

but $G_0 = G_r + iG_i$

$$ImG(0) = \frac{V^2 G_i)}{(w - \varepsilon - V^2 G_r)^2 + (V^2 G_i)^2},$$

with the Green's function G(0) calculated we can obtain the Anderson parameter which is defined by

$$\Gamma = 2\pi V^2 \sum_k \delta(\varepsilon - \varepsilon_k),$$

but the density of states can be defined by

$$\sum_k \delta(\varepsilon - \varepsilon_k) = \frac{-1}{\pi} Im[G(0)],$$

therefore

$$\Gamma = \frac{2\pi V^2}{\pi} Im[G(0)] = \frac{2V^4 G_i}{(w - \varepsilon - V^2 G_r)^2 + (V^2 G_i)^2},$$

we can now calculate the transport coefficient which is defined by

$$\mathcal{L}_n(T) = \frac{1}{h} \int \frac{-\partial n_f(T))}{\partial w} w^n \tau(w) dw,$$

where

$$\tau(w) = -\Gamma Im[G_0(w)] = -\Gamma G_i,$$

this way we have to

$$\mathcal{L}_0(T) = \frac{1}{h} \int \frac{e^{\frac{w}{T}}}{T(e^{\frac{w}{T}} + 1)^2} \frac{2V^4 G_i^2}{(w - \varepsilon - V^2 G_r)^2 + (V^2 G_i)^2} dw,$$

taking $\varepsilon \to 0$

$$\mathcal{L}_0(T) = \frac{1}{h} \int \frac{e^{\frac{w}{T}}}{T(e^{\frac{w}{T}} + 1)^2} \frac{2V^4 G_i^2}{(w - V^2 G_r)^2 + (V^2 G_i)^2} dw.$$

Appendix D

The Kitaev chain Hamiltonian

To understand the SP and SSH chains, it is necessary to introduce some aspects of Majoranas from a simpler model. To this end, we will begin by presenting the Kitaev chain, which is a "toy model" proposed by Kitaev [4]. It is a one-dimensional chain described by the Hamiltonian .

$$H = -\mu \sum_{x=1}^{N} c_x^\dagger c_x - \frac{1}{2} \sum_{x=1}^{N-1} (t c_x^\dagger c_{x+1} + \Delta e^{i\phi} c_x c_{x+1} + t c_{x+1}^\dagger c_x + \Delta e^{-i\phi} c_{x+1}^\dagger c_x^\dagger), \tag{D.1}$$

in terms of the creation and annihilation operators $c^\dagger$ and c, with μ being the chemical potential, t the electron transfer integral between neighboring sites of the chain ("hopping"), Δ the superconducting "gap" with "p" symmetry and ϕ the phase of the superconducting order parameter Δ, with spinless fermions, that is, here we should have a "p" wave-type pairing.

To understand the behavior of the chain we must first define the two operators that describe the Majorana fermions, these are labeled with the subscripts A and B: $\gamma_{A,j}$ and $\gamma_{B,j}$, where the two operators belong to the same site that is represented by the subscript j. We define the operators $\gamma_{A,i}$ and $\gamma_{B,j}$ through their relations with the usual fermionic operators:

$$f = \tfrac{1}{2}(\gamma_A + i\gamma_B),$$
$$f^\dagger = \tfrac{1}{2}(\gamma_A - i\gamma_B).$$

We now relate the operators defined to the above equations to the fermion creation and annihilation operators that define the Kitaev Hamiltonian, c_j and $c_j^\dagger$. Majorana fermions are neutral "particles" of spin 1/2, which have themselves as their antiparticles. Substituting these equations into the commutation relations for fermions:

$$[f, f^\dagger]_+ = 1,$$
$$[f, f]_+ = 0$$

there is

$$[\gamma_{\alpha,i}, \gamma_{\alpha',j}^\dagger]_+ = 2\delta_{\alpha,\alpha'}\delta_{i,j}.$$

Since $\alpha = A, B$, we can then relate them to the creation and annihilation operators that describe the behavior of electrons in the system:

$$c_j = \frac{e^{-\frac{i\phi}{2}}}{2}(\gamma_{A,j} + i\gamma_{B,j}),$$
$$c_j^\dagger = \frac{e^{\frac{i\phi}{2}}}{2}(\gamma_{A,j} - i\gamma_{B,j}).$$

We use the Hamiltonian of Eq. D.1, and by doing some algebraic manipulations, we obtain the Kitaev Hamiltonian as a function of the Majorana fermion operators:

$$H = -\frac{\mu}{2}\sum_{j=1}^{N}(1 + i\gamma_{B,j}\gamma_{A,j}) - \frac{i}{4}\sum_{j=1}^{N-1}[(t+\Delta)(\gamma_{B,j}\gamma_{A,j+1}) - (t-\Delta)(\gamma_{A,j}\gamma_{B,j+1})].$$

We can now analyze some limiting cases. The Kitaev Hamiltonian has three real parameters: the chemical potential μ, the *hopping* between sites and the superconducting pairing Δ. The regime with edge states is obtained when $\Delta = t$ and $\mu = 0$, while the totally trivial regime composed only of ordinary fermions is obtained when $\Delta = t = 0$ and $\mu \neq 0$.

Trivial case:

In this case we have that $\mu \neq 0$ and $t = \Delta = 0$.

$$H = -\frac{\mu}{2}\sum_{j=1}^{N}(1 + i\gamma_{B,j}\gamma_{A,j}), \tag{D.2}$$

we should note that the pairing between MF A and B always occurs at the same site in the chain. The energy spectrum always has a "gap", since it will cost us a finite energy μ to add a spinless electron to the chain. Fig. D.1 illustrates what these interactions would look like.

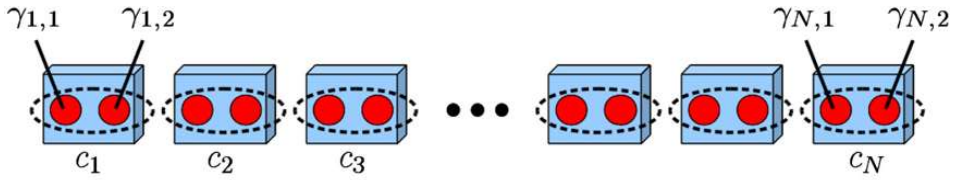

Figure D.1: Trivial case

Topological case:

In this case we have that $\mu = 0$ and $t = \Delta \neq 0$.

$$H = -\frac{it}{2}\sum_{j=1}^{N-1}\gamma_{B,j}\gamma_{A,j+1}. \tag{D.3}$$

we should note that the pairing between MFs A and B always occurs at the neighbours site in the chain. The energy spectrum always has a "gap" also, but now is because of the topological phase, note that has two MFs that is not included in the eq D.3 $\gamma_{A,1}$ and $\gamma_{B,N}$, it is mean that are a state $(-it\gamma_{A,1}\gamma_{B,N})$ with zero energy cost . Fig. D.2 illustrates what these interactions would look like.

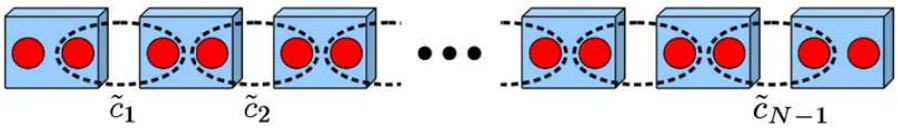

Figure D.2: Topological case

Appendix E

The Falikov-Kimball Hamiltonian

The FK model is a fundamental theoretical model in condensed matter physics that describes systems with two different types of fermion particles: Itinerant (mobile) particles, which can move along the lattice, describing propagating electrons; and localized particles, which are fixed particles, which do not move within the system, representing ions or strongly localized electrons. This section will present more details about the Falikov-Kimball interaction.

A.1 Introduction to the Model

The Falicov-Kimball model, originally formulated in 1969 by Leo Falicov and John Kimball [132], constitutes a fundamental theoretical tool in the study of strongly correlated electronic systems in condensed matter. This model emerges as a remarkable simplification of the Hubbard model while maintaining considerable phenomenological richness that captures the essence of the competition between localized and itinerant electronic states.

The relevance of the model lies precisely in its ability to describe purely electronic phase transitions and localization phenomena that challenge conventional band theory description. The core of the model resides in the local interaction between two distinctive electronic species: itinerant electrons, which propagate freely through the crystal lattice, and localized electrons, which remain confined to specific atomic sites.

A.2 Hamiltonian Formulation

The complete Hamiltonian of the Falicov-Kimball model can be expressed through three fundamental contributions that reflect different aspects of the system's physics:

$$\hat{H}_{FK} = -t \sum_{\langle i,j \rangle} (\hat{c}_i^\dagger \hat{c}_j + \hat{c}_j^\dagger \hat{c}_i) + E_f \sum_i \hat{f}_i^\dagger \hat{f}_i + U \sum_i \hat{c}_i^\dagger \hat{c}_i \hat{f}_i^\dagger \hat{f}_i \tag{E.1}$$

The kinetic term describes the motion of itinerant electrons through the hopping operator between neighboring sites of the crystal lattice. Mathematically, this term is represented by a sum over pairs of first neighbors, thus capturing the nature of electronic propagation in the lattice.

The second term of the Hamiltonian characterizes the energy of localized electrons, incorporating the energy cost associated with the occupation of localized states. This term, proportional to the parameter E_f, largely determines the average density of localized electrons in the system and establishes the energy scale for this electronic species.

The third and most crucial term represents the characteristic interaction of the Falicov-Kimball model: a local repulsive interaction that occurs exclusively when an itinerant electron and a localized electron occupy the same site of the lattice. This interaction, parameterized by the constant U, constitutes the fundamental mechanism through which the most interesting phenomena described by the model emerge.

A.3 The Falicov-Kimball Interaction: Mechanism and Characteristics

The Falicov-Kimball interaction presents distinctive characteristics that differentiate it from other interactions in correlated electronic systems. Its strictly local nature means that the repulsion occurs only when both electronic species coexist at the same atomic site, with no long-range or distance-dependent interaction components.

A fundamental property of this interaction is the dynamic asymmetry between the two electronic species. While itinerant electrons exhibit complete quantum dynamics, with tunneling capability between neighboring sites, localized electrons essentially behave as static quantum impurities. This asymmetry gives the model remarkable mathematical tractability, particularly in the infinite-dimensional limit where it becomes exactly solvable [133].

The interaction establishes a fundamental competition between the kinetic energy associated with the motion of itinerant electrons and the potential energy resulting from local repulsion. When the interaction U dominates over the hopping t, the system develops a tendency toward localization, potentially undergoing transitions to insulating phases. On the other hand, when hopping dominates, metallic behavior prevails and itinerant electrons move almost freely through the lattice.

A.4 Phenomenology Induced by the Interaction

The Falicov-Kimball interaction is responsible for a rich range of physical phenomena that include phase transitions, electronic ordering, and the emergence of correlated phases. One of the most notable phenomena is the correlation-induced metal-insulator transition. For interaction values above a critical value U_c, the energy cost of double occupation becomes prohibitive, effectively suppressing the movement of itinerant electrons and driving the system into a Mott insulating phase.

Another fascinating aspect is the ability of the interaction to promote electronic ordering and

spontaneous breaking of translational symmetry. In certain parameter regimes, localized electrons spontaneously organize into periodic patterns, such as the checkerboard phase or stripe structures, which minimize the global interaction energy by allowing itinerant electrons to avoid sites of high repulsion.

The phase diagram of the model as a function of parameters U/t and electronic densities exhibits considerable complexity, with regions corresponding to metallic, insulating, and ordered phases. The transition between these phases can be continuous or discontinuous, depending on the specific parameter values and the system dimensionality.

A.5 Solubility and Theoretical Treatment

One of the most notable properties of the Falicov-Kimball model is its exact solubility in the infinite-dimensional limit. This characteristic, demonstrated by Ulrich Brandt and collaborators [133], represents a significant advantage over other correlated electron models, such as the Hubbard model, which remains analytically intractable even in this limit.

The solubility in infinite dimension allowed the development of precise theoretical treatments, including the exact construction of the Green's function and the quantitative determination of the phase diagram. More importantly, it served as a fundamental platform for the development of Dynamical Mean Field Theory (DMFT) [134], a powerful tool that revolutionized the study of strongly correlated electron systems.

In finite dimensions, the model is typically studied through advanced numerical methods, such as quantum Monte Carlo simulations, which allow exploration of the effects of quantum fluctuations and the influence of dimensionality on the system's phenomenology.

A.6 Applications and Physical Relevance

The Falicov-Kimball model finds direct application in the description of various real material systems where localized and itinerant electrons coexist. Among the most notable examples are rare-earth compounds, such as TmSe and SmB, where highly localized f-electrons interact with d-conduction electrons, giving rise to complex phenomena such as valence transitions and Kondo behaviors.

In transition metal oxides, such as VO, the model provides valuable insights into the mechanisms of correlation-induced metal-insulator transitions. The model's ability to capture the essence of interaction-induced kinetic blockade makes it particularly suitable for describing these systems.

Beyond these direct applications, the model serves as a theoretical laboratory for exploring fundamental concepts in condensed matter physics, including the role of electronic correlations in transport, the emergence of ordered phases through purely electronic mechanisms, and the nature of quantum phase transitions.

Bibliography

[1] V. Mourik, K. Zuo, S. M. Frolov, S. R. Plissard, E. P. A. M. Bakkers, and L. P. Kouwenhoven. Signatures of majorana fermions in hybrid superconductor-semiconductor nanowire devices. *Science*, 336(6084):1003–1007, 2012.

[2] Stevan Nadj-Perge, Ilya K. Drozdov, Jian Li, Hua Chen, Sangjun Jeon, Jungpil Seo, Allan H. MacDonald, B. Andrei Bernevig, and Ali Yazdani. Observation of majorana fermions in ferromagnetic atomic chains on a superconductor. *Science*, 346(6209):602–607, 2014.

[3] Jason Alicea. New directions in the pursuit of majorana fermions in solid state systems. *Reports on Progress in Physics*, 75(7):076501, Jun 2012.

[4] A Yu Kitaev. Unpaired majorana fermions in quantum wires. *Physics-Uspekhi*, 44(10S):131–136, October 2001.

[5] Yuval Oreg, Gil Refael, and Felix von Oppen. Helical liquids and majorana bound states in quantum wires. *Phys. Rev. Lett.*, 105:177002, Oct 2010.

[6] Roman M. Lutchyn, Jay D. Sau, and S. Das Sarma. Majorana fermions and a topological phase transition in semiconductor-superconductor heterostructures. *Phys. Rev. Lett.*, 105:077001, Aug 2010.

[7] Masatoshi Sato, Yoshiro Takahashi, and Satoshi Fujimoto. Non-abelian topological order in s-wave superfluids of ultracold fermionic atoms. *Phys. Rev. Lett.*, 103:020401, Jul 2009.

[8] Riku Tuovinen, Enrico Perfetto, Robert van Leeuwen, Gianluca Stefanucci, and Michael A Sentef. Distinguishing majorana zero modes from impurity states through time-resolved transport. *New Journal of Physics*, 21(10):103038, October 2019.

[9] Chun-Xiao Liu, Jay D. Sau, Tudor D. Stanescu, and S. Das Sarma. Andreev bound states versus majorana bound states in quantum dot-nanowire-superconductor hybrid structures: Trivial versus topological zero-bias conductance peaks. *Phys. Rev. B*, 96:075161, Aug 2017.

[10] Elsa Prada, Pablo San-Jose, Michiel W. A. de Moor, Attila Geresdi, Eduardo J. H. Lee, Jelena Klinovaja, Daniel Loss, Jesper Nygård, Ramón Aguado, and Leo P. Kouwenhoven. From andreev

to majorana bound states in hybrid superconductor–semiconductor nanowires. *Nature Reviews Physics*, 2(10):575–594, Oct 2020.

[11] Bao-Zong Wang, Yue-Hui Lu, Wei Sun, Shuai Chen, Youjin Deng, and Xiong-Jun Liu. Dirac-, rashba-, and weyl-type spin-orbit couplings: Toward experimental realization in ultracold atoms. *Physical Review A*, 97(1), January 2018.

[12] Hao Zhang, Chun-Xiao Liu, Sasa Gazibegovic, Di Xu, John A. Logan, Guanzhong Wang, Nick van Loo, Jouri D. S. Bommer, Michiel W. A. de Moor, Diana Car, Roy L. M. Op het Veld, Petrus J. van Veldhoven, Sebastian Koelling, Marcel A. Verheijen, Mihir Pendharkar, Daniel J. Pennachio, Borzoyeh Shojaei, Joon Sue Lee, Chris J. Palmstrøm, Erik P. A. M. Bakkers, S. Das Sarma, and Leo P. Kouwenhoven. Retracted article: Quantized majorana conductance. *Nature*, 556(7699):74–79, March 2018.

[13] Hao Zhang, Chun-Xiao Liu, Sasa Gazibegovic, Di Xu, John A. Logan, Guanzhong Wang, Nick van Loo, Jouri D. S. Bommer, Michiel W. A. de Moor, Diana Car, Roy L. M. Op het Veld, Petrus J. van Veldhoven, Sebastian Koelling, Marcel A. Verheijen, Mihir Pendharkar, Daniel J. Pennachio, Borzoyeh Shojaei, Joon Sue Lee, Chris J. Palmstrøm, Erik P. A. M. Bakkers, S. Das Sarma, and Leo P. Kouwenhoven. Retracted article: Quantized majorana conductance. *Nature*, 556(7699):74–79, Apr 2018.

[14] Morteza Aghaee, Alejandro Alcaraz Ramirez, Zulfi Alam, Rizwan Ali, Mariusz Andrzejczuk, Andrey Antipov, Mikhail Astafev, Amin Barzegar, Bela Bauer, Jonathan Becker, Umesh Kumar Bhaskar, Alex Bocharov, Srini Boddapati, David Bohn, Jouri Bommer, Leo Bourdet, Arnaud Bousquet, Samuel Boutin, Lucas Casparis, Benjamin J. Chapman, Sohail Chatoor, Anna Wulff Christensen, Cassandra Chua, Patrick Codd, William Cole, Paul Cooper, Fabiano Corsetti, Ajuan Cui, Paolo Dalpasso, Juan Pablo Dehollain, Gijs de Lange, Michiel de Moor, Andreas Ekefjärd, Tareq El Dandachi, Juan Carlos Estrada Saldaña, Saeed Fallahi, Luca Galletti, Geoff Gardner, Deshan Govender, Flavio Griggio, Ruben Grigoryan, Sebastian Grijalva, Sergei Gronin, Jan Gukelberger, Marzie Hamdast, Firas Hamze, Esben Bork Hansen, Sebastian Heedt, Zahra Heidarnia, Jesús Herranz Zamorano, Samantha Ho, Laurens Holgaard, John Hornibrook, Jinnapat Indrapiromkul, Henrik Ingerslev, Lovro Ivancevic, Thomas Jensen, Jaspreet Jhoja, Jeffrey Jones, Konstantin V. Kalashnikov, Ray Kallaher, Rachpon Kalra, Farhad Karimi, Torsten Karzig, Evelyn King, Maren Elisabeth Kloster, Christina Knapp, Dariusz Kocon, Jonne V. Koski, Pasi Kostamo, Mahesh Kumar, Tom Laeven, Thorvald Larsen, Jason Lee, Kyunghoon Lee, Grant Leum, Kongyi Li, Tyler Lindemann, Matthew Looij, Julie Love, Marijn Lucas, Roman Lutchyn, Morten Hannibal Madsen, Nash Madulid, Albert Malmros, Michael Manfra, Devashish Mantri, Signe Brynold Markussen, Esteban Martinez, Marco Mattila, Robert McNeil, Antonio B. Mei, Ryan V. Mishmash, Gopakumar Mohandas, Christian Mollgaard, Trevor Morgan, George Moussa, Chetan Nayak, Jens Hedegaard Nielsen, Jens Munk Nielsen, William Hvidtfelt Padkar Nielsen, Bas Nijholt, Mike Nystrom, Eoin

O'Farrell, Thomas Ohki, Keita Otani, Brian Paquelet Wütz, Sebastian Pauka, Karl Petersson, Luca Petit, Dima Pikulin, Guen Prawiroatmodjo, Frank Preiss, Eduardo Puchol Morejon, Mohana Rajpalke, Craig Ranta, Katrine Rasmussen, David Razmadze, Outi Reentila, David J. Reilly, Yuan Ren, Ken Reneris, Richard Rouse, Ivan Sadovskyy, Lauri Sainiemi, Irene Sanlorenzo, Emma Schmidgall, Cristina Sfiligoj, Mustafeez Bashir Shah, Kevin Simoes, Shilpi Singh, Sarat Sinha, Thomas Soerensen, Patrick Sohr, Tomas Stankevic, Lieuwe Stek, Eric Stuppard, Henri Suominen, Judith Suter, Sam Teicher, Nivetha Thiyagarajah, Raj Tholapi, Mason Thomas, Emily Toomey, Josh Tracy, Michelle Turley, Shivendra Upadhyay, Ivan Urban, Kevin Van Hoogdalem, David J. Van Woerkom, Dmitrii V. Viazmitinov, Dominik Vogel, John Watson, Alex Webster, Joseph Weston, Georg W. Winkler, Di Xu, Chung Kai Yang, Emrah Yucelen, Roland Zeisel, Guoji Zheng, Justin Zilke, and Microsoft Azure Quantum. Interferometric single-shot parity measurement in inas–al hybrid devices. *Nature*, 638(8051):651–655, Feb 2025.

[15] R. M. Lutchyn, E. P. A. M. Bakkers, L. P. Kouwenhoven, P. Krogstrup, C. M. Marcus, and Y. Oreg. Majorana zero modes in superconductor–semiconductor heterostructures. *Nature Reviews Materials*, 3(5):52–68, May 2018.

[16] C. W. J. Beenakker. Universal limit of critical-current fluctuations in mesoscopic josephson junctions. *Phys. Rev. Lett.*, 67:3836–3839, Dec 1991.

[17] E. Vernek, P. H. Penteado, A. C. Seridonio, and J. C. Egues. Subtle leakage of a majorana mode into a quantum dot. *Phys. Rev. B*, 89:165314, Apr 2014.

[18] M. T. Deng, S. Vaitiekėnas, E. B. Hansen, J. Danon, M. Leijnse, K. Flensberg, J. Nygård, P. Krogstrup, and C. M. Marcus. Majorana bound state in a coupled quantum-dot hybrid-nanowire system. *Science*, 354(6319):1557–1562, December 2016.

[19] Sankar Das Sarma and Haining Pan. Disorder-induced zero-bias peaks in majorana nanowires. *Phys. Rev. B*, 103:195158, May 2021.

[20] Dong E. Liu and Harold U. Baranger. Detecting a majorana-fermion zero mode using a quantum dot. *Phys. Rev. B*, 84:201308, Nov 2011.

[21] L. M. Falicov and J. C. Kimball. Simple model for semiconductor-metal transitions: Smb_6 and transition-metal oxides. *Phys. Rev. Lett.*, 22:997–999, May 1969.

[22] Masatoshi Sato and Yoichi Ando. Topological superconductors: a review. *Reports on Progress in Physics*, 80(7):076501, may 2017.

[23] M M Sharma, Prince Sharma, N K Karn, and V P S Awana. Comprehensive review on topological superconducting materials and interfaces. *Superconductor Science and Technology*, 35(8):083003, July 2022.

[24] Oliver Breunig and Yoichi Ando. Opportunities in topological insulator devices. *Nature Reviews Physics*, 4(3):184–193, December 2021.

[25] Jacob Linder and Jason W. A. Robinson. Superconducting spintronics. *Nature Physics*, 11(4):307–315, Apr 2015.

[26] Chetan Nayak, Steven H. Simon, Ady Stern, Michael Freedman, and Sankar Das Sarma. Non-abelian anyons and topological quantum computation. *Rev. Mod. Phys.*, 80:1083–1159, Sep 2008.

[27] Jason Alicea, Yuval Oreg, Gil Refael, Felix von Oppen, and Matthew P. A. Fisher. Non-abelian statistics and topological quantum information processing in 1d wire networks. *Nature Physics*, 7(5):412–417, February 2011.

[28] Po-Hao Chou, Chia-Hsin Chen, Shih-Wei Liu, Chung-Hou Chung, and Chung-Yu Mou. Geometry-induced topological superconductivity. *Phys. Rev. B*, 103:014508, Jan 2021.

[29] Haining Pan and Sankar Das Sarma. Majorana nanowires, kitaev chains, and spin models. *Phys. Rev. B*, 107:035440, Jan 2023.

[30] Morteza Aghaee, Arun Akkala, Zulfi Alam, Rizwan Ali, Alejandro Alcaraz Ramirez, Mariusz Andrzejczuk, Andrey E. Antipov, Pavel Aseev, Mikhail Astafev, Bela Bauer, Jonathan Becker, Srini Boddapati, Frenk Boekhout, Jouri Bommer, Tom Bosma, Leo Bourdet, Samuel Boutin, Philippe Caroff, Lucas Casparis, Maja Cassidy, Sohail Chatoor, Anna Wulf Christensen, Noah Clay, William S. Cole, Fabiano Corsetti, Ajuan Cui, Paschalis Dalampiras, Anand Dokania, Gijs de Lange, Michiel de Moor, Juan Carlos Estrada Saldaña, Saeed Fallahi, Zahra Heidarnia Fathabad, John Gamble, Geoff Gardner, Deshan Govender, Flavio Griggio, Ruben Grigoryan, Sergei Gronin, Jan Gukelberger, Esben Bork Hansen, Sebastian Heedt, Jesús Herranz Zamorano, Samantha Ho, Ulrik Laurens Holgaard, Henrik Ingerslev, Linda Johansson, Jeffrey Jones, Ray Kallaher, Farhad Karimi, Torsten Karzig, Evelyn King, Maren Elisabeth Kloster, Christina Knapp, Dariusz Kocon, Jonne Koski, Pasi Kostamo, Peter Krogstrup, Mahesh Kumar, Tom Laeven, Thorvald Larsen, Kongyi Li, Tyler Lindemann, Julie Love, Roman Lutchyn, Morten Hannibal Madsen, Michael Manfra, Signe Markussen, Esteban Martinez, Robert McNeil, Elvedin Memisevic, Trevor Morgan, Andrew Mullally, Chetan Nayak, Jens Nielsen, William Hvidtfelt Padkær Nielsen, Bas Nijholt, Anne Nurmohamed, Eoin O'Farrell, Keita Otani, Sebastian Pauka, Karl Petersson, Luca Petit, Dmitry I. Pikulin, Frank Preiss, Marina Quintero-Perez, Mohana Rajpalke, Katrine Rasmussen, Davydas Razmadze, Outi Reentila, David Reilly, Richard Rouse, Ivan Sadovskyy, Lauri Sainiemi, Sydney Schreppler, Vadim Sidorkin, Amrita Singh, Shilpi Singh, Sarat Sinha, Patrick Sohr, Toma š Stankevič, Lieuwe Stek, Henri Suominen, Judith Suter, Vicky Svidenko, Sam Teicher, Mine Temuerhan, Nivetha Thiyagarajah, Raj Tholapi, Mason Thomas, Emily Toomey, Shivendra Upadhyay, Ivan Urban, Saulius Vaitiekėnas, Kevin Van Hoogdalem, David Van Woerkom, Dmitrii V. Viazmitinov, Dominik Vogel, Steven Waddy, John Watson, Joseph Weston, Georg W. Winkler, Chung Kai Yang,

Sean Yau, Daniel Yi, Emrah Yucelen, Alex Webster, Roland Zeisel, and Ruichen Zhao. Inas-al hybrid devices passing the topological gap protocol. *Phys. Rev. B*, 107:245423, Jun 2023.

[31] Jay D. Sau, Roman M. Lutchyn, Sumanta Tewari, and S. Das Sarma. Generic new platform for topological quantum computation using semiconductor heterostructures. *Phys. Rev. Lett.*, 104:040502, Jan 2010.

[32] Jay D. Sau, Sumanta Tewari, Roman M. Lutchyn, Tudor D. Stanescu, and S. Das Sarma. Nonabelian quantum order in spin-orbit-coupled semiconductors: Search for topological majorana particles in solid-state systems. *Phys. Rev. B*, 82:214509, Dec 2010.

[33] Sumanta Tewari, T. D. Stanescu, Jay D. Sau, and S. Das Sarma. Topological minigap in quasi-one-dimensional spin-orbit-coupled semiconductor majorana wires. *Phys. Rev. B*, 86:024504, Jul 2012.

[34] T D Stanescu and S Tewari. Majorana fermions in semiconductor nanowires: fundamentals, modeling, and experiment. *Journal of Physics: Condensed Matter*, 25(23):233201, May 2013.

[35] R. C. Bento Ribeiro, J. H. Correa, L. S. Ricco, A. C. Seridonio, and M. S. Figueira. Spin-polarized majorana zero modes in double zigzag honeycomb nanoribbons. *Phys. Rev. B*, 105:205115, May 2022.

[36] A Bhattacharyya, D T Adroja, Y Feng, Debarchan Das, P K Biswas, Tanmoy Das, and J. Zhao. μsr study of unconventional pairing symmetry in the quasi-1d $na_2cr_3as_3$ superconductor, 2021.

[37] Eva Liebhaber, Lisa M. Rütten, Gaël Reecht, Jacob F. Steiner, Sebastian Rohlf, Kai Rossnagel, Felix von Oppen, and Katharina J. Franke. Quantum spins and hybridization in artificially-constructed chains of magnetic adatoms on a superconductor. *Nature Communications*, 13(1), April 2022.

[38] E. Dumitrescu and Sumanta Tewari. Topological properties of the time-reversal-symmetric kitaev chain and applications to organic superconductors. *Phys. Rev. B*, 88:220505, Dec 2013.

[39] Niklas M. Gergs, Lars Fritz, and Dirk Schuricht. Topological order in the kitaev/majorana chain in the presence of disorder and interactions. *Phys. Rev. B*, 93:075129, Feb 2016.

[40] Stephan Rachel. Interacting topological insulators: a review. *Reports on Progress in Physics*, 81(11):116501, oct 2018.

[41] Giovanni Nunziante, Alfonso Maiellaro, Claudio Guarcello, and Roberta Citro. Topological Phase Diagram of an Interacting Kitaev Chain: Mean Field versus DMRG Study. *Condens. Mat.*, 9(1):20, 2024.

[42] Yiting Deng and Yan He. Exact solutions of topological superconductor model with hubbard interactions, 2021.

[43] Max McGinley, Johannes Knolle, and Andreas Nunnenkamp. Robustness of majorana edge modes and topological order: Exact results for the symmetric interacting kitaev chain with disorder. *Phys. Rev. B*, 96:241113, Dec 2017.

[44] Haining Pan and S. Das Sarma. Disorder effects on majorana zero modes: Kitaev chain versus semiconductor nanowire. *Phys. Rev. B*, 103:224505, Jun 2021.

[45] Simon Lieu, Derek K. K. Lee, and Johannes Knolle. Disorder protected and induced local zero-modes in longer-range kitaev chains. *Phys. Rev. B*, 98:134507, Oct 2018.

[46] Guang Yang and D. E. Feldman. Exact zero modes and decoherence in systems of interacting majorana fermions. *Phys. Rev. B*, 89:035136, Jan 2014.

[47] Armin Rahmani and Marcel Franz. Interacting majorana fermions. *Reports on Progress in Physics*, 82(8):084501, July 2019.

[48] Christian Prosko, Shu-Ping Lee, and Joseph Maciejko. Simple z_2 lattice gauge theories at finite fermion density. *Phys. Rev. B*, 96:205104, Nov 2017.

[49] C. Gruber, D. Ueltschi, and J. Jędrzejewski. Molecule formation and the farey tree in the one-dimensional falicov-kimball model. *Journal of Statistical Physics*, 76(1–2):125–157, July 1994.

[50] Wade DeGottardi, Diptiman Sen, and Smitha Vishveshwara. Topological phases, majorana modes and quench dynamics in a spin ladder system. *New Journal of Physics*, 13(6):065028, June 2011.

[51] Bernard Derrida, K. Mecheri, and Jean-Louis Pichard. Lyapounov exponents of products of random matrices : weak disorder expansion. - application to localisation. *http://dx.doi.org/10.1051/jphys:01987004805073300*, 48, 05 1987.

[52] Wade DeGottardi, Manisha Thakurathi, Smitha Vishveshwara, and Diptiman Sen. Majorana fermions in superconducting wires: Effects of long-range hopping, broken time-reversal symmetry, and potential landscapes. *Phys. Rev. B*, 88:165111, Oct 2013.

[53] Boris Narozhny. Majorana fermions in the nonuniform ising-kitaev chain: exact solution. *Scientific Reports*, 7(1):1447, May 2017.

[54] A C P Lima, M S Figueira, and Mucio A Continentino. Interplay between topology and interactions in superconducting chains. *Journal of Physics: Condensed Matter*, 37(35):355601, aug 2025.

[55] Polozine Alexandre, Sirotinskaya Susanna, and Schaeffer Lírio. History of development of thermoelectric materials for electric power generation and criteria of their quality. *Materials Research*, 17:1260, June 2014.

[56] A F Iofee. *Semiconductor Thermoelements and Thermoelectric Cooling*. Infosearch, London, 1 edition, 1957.

[57] D. A. Wright. Thermoelectric properties of bismuth telluride and its alloys. *Nature*, 181(4612):834–834, Mar 1958.

[58] A F Joffe and L S Stil. Physical problems of thermoelectricity. *Reports on Progress in Physics*, 22:167, 1959.

[59] Ian T. Witting, Thomas C. Chasapis, Francesco Ricci, Matthew Peters, Nicholas A. Heinz, Geoffroy Hautier, and G. Jeffrey Snyder. The thermoelectric properties of bismuth telluride. *Advanced Electronic Materials*, 5(6):1800904, 2019.

[60] Ning Xu, Yong Xu, and Jia Zhu. Topological insulators for thermoelectrics. *npj Quantum Materials*, 2(1):51, Sep 2017.

[61] Ke-Jun Xu, Su-Di Chen, Yu He, Junfeng He, Shujie Tang, Chunjing Jia, Eric Yue Ma, Sung-Kwan Mo, Donghui Lu, Makoto Hashimoto, Thomas P. Devereaux, and Zhi-Xun Shen. Metallic surface states in a correlated d-electron topological kondo insulator candidate fesb2. *Proceedings of the National Academy of Sciences*, 117(27):15409–15413, 2020.

[62] Johannes Gooth, Gabi Schierning, Claudia Felser, and Kornelius Nielsch. Quantum materials for thermoelectricity. *MRS Bull.*, 43(3):187–192, 2018.

[63] Aurelien Manchon, Hyun Cheol Koo, Junsaku Nitta, SM Frolov, and RA Duine. New perspectives for rashba spin-orbit coupling. *Nat. Mater.*, 14:871, 2015.

[64] Mujeeb Ahmad, Khushboo Agarwal, and B. R. Mehta. An anomalously high seebeck coefficient and power factor in ultrathin bi2te3 film: Spin–orbit interaction. *J. Appl. Phys.*, 128:035108, 2020.

[65] Ryuji Takahashi and Shuichi Murakami. Thermoelectric transport in topological insulators. *Semicond. Sci. Technol.*, 27:124005, 2012.

[66] M. Cassinelli, S. Müller, K.-O. Voss, C. Trautmann, F. Völklein, J. Gooth, K. Nielsch, and M. E. Toimil-Molares. Influence of surface states and size effects on the seebeck coefficient and electrical resistance of bi1xsbx nanowire arrays. *Nanoscale*, 9:3169, 2017.

[67] Jinghua Liang, Long Cheng, Jie Zhang, Huijun Liu, and Zhenyu Zhang. Maximizing the thermoelectric performance of topological insulator bi2te3 films in the few-quintuple layer regime. *Nanoscale*, 8:8855–8862, 2016.

[68] P. Fernández-Yanez, V. Romero, O. Armas, and G. Cerretti. Thermal management of thermoelectric generators for waste energy recovery. *Applied Thermal Engineering*, 196:117291, 2021.

[69] N. P. Armitage, E. J. Mele, and Ashvin Vishwanath. Weyl and dirac semimetals in three-dimensional solids. *Rev. Mod. Phys.*, 90:015001, Jan 2018.

[70] János K Asbóth, László Oroszlány, and András Pályi. A short course on topological insulators. *Lecture notes in physics*, 919:166, 2016.

[71] F. Buccheri, A. Nava, R. Egger, P. Sodano, and D. Giuliano. Violation of the wiedemann-franz law in the topological kondo model, 2021.

[72] Xiao-Liang Qi and Shou-Cheng Zhang. Topological insulators and superconductors. *Rev. Mod. Phys.*, 83:1057–1110, Oct 2011.

[73] Jing Wang and Shou-Cheng Zhang. Topological states of condensed matter. *Nature Materials*, 16(11):1062–1067, 2017.

[74] Haining Pan, Jay D. Sau, and S. Das Sarma. Three-terminal nonlocal conductance in majorana nanowires: Distinguishing topological and trivial in realistic systems with disorder and inhomogeneous potential. *Phys. Rev. B*, 103:014513, Jan 2021.

[75] Takeshi Mizushima, Yasumasa Tsutsumi, Masatoshi Sato, and Kazushige Machida. Symmetry protected topological superfluid3he-b. *Journal of Physics: Condensed Matter*, 27(11):113203, mar 2015.

[76] Shun-Qing Shen. *Springer Series in Solid-State Sciences 187 Topological Insulators Dirac Equation in Condensed Matter Second Edition*, volume 187 of *Springer Series in Solid-State Sciences*. Springer Singapore, Singapore, 2017.

[77] M. Z. Hasan and C L Kane. Colloquium: Topological insulators. *Rev. Mod. Phys.*, 82(4):3045–3067, 2010.

[78] Mucio A. Continentino, Heron Caldas, David Nozadze, and Nandini Trivedi. Topological states in normal and superconducting p-wave chains. *Phys. Lett. Sect. A Gen. At. Solid State Phys.*, 378(45):3340–3347, 2014.

[79] Symmetry protected topological superfluid3he-b. *Journal of Physics: Condensed Matter*, 27(11):113203, mar 2015.

[80] Vasilii I. Artyukhov, Mingjie Liu, and Boris I. Yakobson. Mechanically induced metal–insulator transition in carbyne. *Nano Letters*, 14(8):4224–4229, 08 2014.

[81] Bitao Pan, Jun Xiao, Jiling Li, Pu Liu, Chengxin Wang, and Guowei Yang. Carbyne with finite length: The one-dimensional sp carbon. *Science Advances*, 138(9):1106–1109, 2015.

[82] Qiang Sun, Liangliang Cai, Shiyong Wang, Roland Widmer, Huanxin Ju, Junfa Zhu, Lei Li, Yunbin He, Pascal Ruffieux, Roman Fasel, and Wei Xu. Bottom-up synthesis of metalated carbyne. *Journal of the American Chemical Society*, 138(4):1106–1109, 2016.

[83] Lei Shi, Philip Rohringer, Kazu Suenaga, Yoshiko Niimi, Jani Kotakoski, Jannik C. Meyer, Herwig Peterlik, Marius Wanko, Seymur Cahangirov, Angel Rubio, Zachary J. Lapin, Lukas Novotny, Paola Ayala, and Thomas Pichler. Confined linear carbon chains as a route to bulk carbyne. *Nature Materials*, 15(6):634–639, 2016.

[84] A.C.L.B. Lustosa, M. Evers, D.F. Franceschini, F.J. Litterst, and Yutao Xing. sp-hybridized carbon atoms formed by low-energy collisions in carbon nanofoams produced by pulsed laser deposition. *Materials Letters*, 314:131886, 2022.

[85] W. P. Su, J. R. Schrieffer, and A. J. Heeger. Soliton excitations in polyacetylene. *Phys. Rev. B*, 22:2099–2111, Aug 1980.

[86] Van Dong Pham, Yi Pan, Steven C Erwin, Felix von Oppen, Kiyoshi Kanisawa, and Stefan Fölsch. Topological states in dimerized quantum-dot chains created by atom manipulation. *arXiv preprint arXiv:2112.00801*, 2021.

[87] M. J. Rice and E. J. Mele. Elementary excitations of a linearly conjugated diatomic polymer. *Phys. Rev. Lett.*, 49:1455 – 1459, Nov 1982.

[88] N. R. Cooper, J. Dalibard, and I. B. Spielman. Topological bands for ultracold atoms. *Rev. Mod. Phys.*, 91:015005, Mar 2019.

[89] E-Ni Foo, M.F. Thorpe, and D. Weaire. Effective surface potential method for calculating surface states. *Surface Science*, 57(1):323–347, 1976.

[90] Martin T Maurer, Yen-Ting Lin, Dante M Kennes, Mikhail Pletyukhov, Herbert Schoeller, and Volker Meden. A quantum dot coupled to topological insulators: the role of edge states. *arXiv preprint arXiv:2112.11814*, 2021.

[91] Linhu Li, Zhihao Xu, and Shu Chen. Topological phases of generalized su-schrieffer-heeger models. *Phys. Rev. B*, 89:085111, Feb 2014.

[92] Han-Ting Chen, Chia-Hsun Chang, and Hsien chung Kao. Connection between the winding number and the chern number. *Chinese Journal of Physics*, 72:50–68, 2021.

[93] W. P. Su, J. R. Schrieffer, and A. J. Heeger. Solitons in polyacetylene. *Phys. Rev. Lett.*, 42:1698–1701, Jun 1979.

[94] A. O. Gogolin, A. M. Tsvelik, and A. A. Nersesyan. *Bosonization and Strongly Correlated Systems.* Cambridge University Press, 1998.

[95] A. A. Belavin, A. M. Polyakov, and A. B. Zamolodchikov. Infinite conformal symmetry in two-dimensional quantum field theory. *Nuclear Physics B*, 241(2):333–380, 1984.

[96] Pasquale Calabrese and John Cardy. Entanglement entropy and quantum field theory. *Journal of Statistical Mechanics: Theory and Experiment*, 2004(06):P06002, 2004.

[97] P. C. Vlaar and R. Verresen. Finite-size scaling of entanglement entropy at the (1+1)d conformal quantum critical point. *arXiv preprint*, 2022.

[98] Frank Pollmann and Ari M. Turner. Detection of symmetry-protected topological phases in one dimension. *Physical Review B*, 86(12):125441, 2012.

[99] J. M. Luttinger. Theory of thermal transport coefficients. *Physical Review*, 135(6A):A1505–A1514, 1964.

[100] J. L. Tomazelli and R. C. Di Lorenzo. Central charge and thermal conductance in quantum hall systems. *Physical Review B*, 73(8):085304, 2006.

[101] C. L. Kane and Matthew P. A. Fisher. Thermal transport in a luttinger liquid. *Physical Review Letters*, 76(17):3192–3195, 1996.

[102] Y. O. Nakagawa, M. Watanabe, H. Fujita, and M. Oshikawa. Uniqueness of the universal conductivity at conformal quantum critical points. *Physical Review B*, 98(11):115147, 2018.

[103] M. Yoshida, A. C. Seridonio, and L. N. Oliveira. Universal zero-bias conductance for the single-electron transistor. *Phys. Rev. B*, 80:235317, Dec 2009.

[104] Mariana M. Odashima, Beatriz G. Prado, and E. Vernek. Pedagogical introduction to equilibrium Green's functions: condensed-matter examples with numerical implementations. *Rev. Bras. Ensino Física*, 39(1):1–26, sep 2016.

[105] L. S. Ricco, F. A. Dessotti, I. A. Shelykh, M. S. Figueira, and A. C. Seridonio. Tuning of heat and charge transport by majorana fermions. *Scientific Reports*, 8(1):2790, 2018.

[106] G D Mahan and J O Sofo. The best thermoelectric. *Proceedings of the National Academy of Sciences*, 93(15):7436–7439, 1996.

[107] D. Giuliano, A. Nava, R. Egger, P. Sodano, and F. Buccheri. Multi-particle scattering and breakdown of the wiedemann-franz law at a junction of n interacting quantum wires, 2021.

[108] S. N. Kempkes, A. Quelle, and C. Morais Smith. Universalities of thermodynamic signatures in topological phases. *Scientific Reports*, 6(1):38530, 2016.

[109] P. M. Chaikin. *An Introduction to Thermopower for Those Who Might Want to Use It to Study Organic Conductors and Superconductors*, pages 101–115. Springer US, Boston, MA, 1990.

[110] Michael R. Peterson and B. Sriram Shastry. Kelvin formula for thermopower. *Phys. Rev. B*, 82:195105, Nov 2010.

[111] Y.-T. Lin, D. M. Kennes, M. Pletyukhov, C. S. Weber, H. Schoeller, and V. Meden. Interacting rice-mele model: Bulk and boundaries. *Phys. Rev. B*, 102:085122, Aug 2020.

[112] S. Rufo, Nei Lopes, Mucio A. Continentino, and M. A. R. Griffith. Multicritical behavior in topological phase transitions. *Phys. Rev. B*, 100:195432, Nov 2019.

[113] S. Rufo, M. A. R. Griffith, Nei Lopes, and Mucio A. Continentino. Anisotropic scaling for 3d topological models. *Scientific Reports*, 11(1):22524, NOV 18 2021.

[114] Adam Rycerz. Wiedemann–franz law for massless dirac fermions with implications for graphene. *Materials*, 14(11), 2021.

[115] Piotr Majek, Krzysztof P. Wójcik, and Ireneusz Weymann. Spin-resolved thermal signatures of majorana-kondo interplay in double quantum dots. *Physical Review B*, 105(7), Feb 2022.

[116] Björn Kubala, Jürgen König, and Jukka Pekola. Violation of the wiedemann-franz law in a single-electron transistor. *Phys. Rev. Lett.*, 100:066801, Feb 2008.

[117] Giuliano Benenti, Giulio Casati, Keiji Saito, and Robert S. Whitney. Fundamental aspects of steady-state conversion of heat to work at the nanoscale. *Physics Reports*, 694:1–124, 2017.

[118] Artis Svilans, Martin Josefsson, Adam M. Burke, Sofia Fahlvik, Claes Thelander, Heiner Linke, and Martin Leijnse. Thermoelectric characterization of the kondo resonance in nanowire quantum dots. *Phys. Rev. Lett.*, 121:206801, Nov 2018.

[119] Bivas Dutta, Danial Majidi, Alvaro García Corral, Paolo A. Erdman, Serge Florens, Theo A. Costi, Hervé Courtois, and Clemens B. Winkelmann. Direct probe of the seebeck coefficient in a kondo-correlated single-quantum-dot transistor. *Nano Letters*, 19(1):506–511, 2019.

[120] *Universal zero-bias conductance for the single-electron transistor*, volume 80. American Physical Society, 2009.

[121] Gordon W Semenoff and Pasquale Sodano. Stretched quantum states emerging from a majorana medium. *Journal of Physics B: Atomic, Molecular and Optical Physics*, 40(8):1479–1488, mar 2007.

[122] Suzanne C. Bart. What is the "lanthanide contraction"? *Inorganic Chemistry*, 62(9):3713–3714, 2023. PMID: 36812147.

[123] SHUN-QING SHEN, WEN-YU SHAN, and HAI-ZHOU LU. Topological insulator and the dirac equation. *SPIN*, 01(01):33–44, June 2011.

[124] Wade DeGottardi, Diptiman Sen, and Smitha Vishveshwara. Majorana fermions in superconducting 1d systems having periodic, quasiperiodic, and disordered potentials. *Phys. Rev. Lett.*, 110:146404, Apr 2013.

[125] A. Altland and B.D. Simons. *Condensed Matter Field Theory*. Cambridge University Press, 2010.

[126] Abhijeet Alase. *Boundary Physics and Bulk-Boundary Correspondence in Topological Phases of Matter*. PhD thesis, Dartmouth College, New Hampshire, January 2019.

[127] A C P Lima, R C Bento Ribeiro, J H Correa, Fernanda Deus, M S Figueira, and Mucio A Continentino. Thermoelectric properties of topological chains coupled to a quantum dot. *Scientific Reports*, 13(1):1508, January 2023.

[128] Kenta Esaki, Masatoshi Sato, Kazuki Hasebe, and Mahito Kohmoto. Edge states and topological phases in non-hermitian systems. *Phys. Rev. B*, 84:205128, Nov 2011.

[129] Emil J. Bergholtz, Jan Carl Budich, and Flore K. Kunst. Exceptional topology of non-hermitian systems. *Rev. Mod. Phys.*, 93:015005, Feb 2021.

[130] Shunyu Yao and Zhong Wang. Edge states and topological invariants of non-hermitian systems. *Phys. Rev. Lett.*, 121:086803, Aug 2018.

[131] Alfonso Maiellaro, Francesco Romeo, and Roberta Citro. Topological phase diagram of a kitaev ladder. *The European Physical Journal Special Topics*, 227(12):1397–1404, Dec 2018.

[132] Leopoldo M Falicov and John C Kimball. Simple model for semiconductor-metal transitions: Smb

–

6 and transition-metal oxides. *Physical Review Letters*, 22(19):997, 1969.

[133] U Brandt and R Schmidt. Exact results for the falicov-kimball model in the limit of infinite dimensions. *Zeitschrift für Physik B Condensed Matter*, 67(1):43–53, 1989.

[134] JK Freericks and V Zlatić. Exact dynamical mean-field theory of the falicov-kimball model. *Reviews of Modern Physics*, 75(4):1333, 2003.